University of Stavanger

Faculty of Science and Technology

MASTER'S THESIS

Study program/ Specialization: Petroleum Engineering/ Reservoir Engineering	Spring Semester 2018 Open
Author: Siri Sandvik	..... Writer's Signature
Faculty Supervisor: Pål Østebø Andersen Co-supervisors: Skule Strand and Arild Lohne	
Title of Thesis: **Simulation of oil recovery by wettability alteration – interpretation of Smart water imbibition experiments at reservoir conditions**	
Credits (ECTS): 30	
Key Words: Spontaneous Imbibition Smart Water Wettability Alteration Simulation IORCoreSim	Pages: 71 + Enclosure: 0 Stavanger June 14, 2018

This page is intentionally left blank

Acknowledgments

First and foremost, I would like to express my gratitude towards my supervisor, Dr. Pål Østebø Andersen, for letting me work on such an exciting and challenging thesis. This thesis would not have been possible without his cheerful attitude and constant source of encouragement. I am very grateful for his commitment and continuous support throughout the last semester.

I would also like to express my sincere gratitude towards my co-supervisors, Sr. Research Engineer Arild Lohne and Prof. Skule Strand, for their professional knowledge and valuable discussions. Their mentoring and encouragement are highly appreciated.

Finally, I would like to express my thankfulness towards Prof. Aksel Hiorth for his professional advices and constructive feedback during the work of this thesis.

This page is intentionally left blank

Abstract

More than 50 % of the proven oil resources in the world are present in carbonates, but the recovery rate is relatively low. Accordingly, a lot of focus has been on improving the efficiency of carbonate reservoirs by applying enhanced oil recovery (EOR) methods. Since most of the fractured carbonate reservoirs are oil-wet, the reservoir rock will hold more strongly onto the oil compared to a water-wet rock. Spontaneous imbibition (SI) of Smart water is the main recovery mechanism in carbonate reservoirs, where a wettability alteration towards a more water-wet rock takes place. When Smart water spontaneously imbibes into a chalk core, SO_4^{2-} will adsorb onto the positive water-wet surface sites, whereas Ca^{2+} complexes with carboxylates in the oil. Subsequently, some of the organic materials are released from the surface and contributes to a higher oil recovery.

Several analytical and numerical models have been developed to describe the SI process in carbonate reservoirs. The models aim to capture the complex interactions between the imbibing Smart water, crude oil, formation water and the rock surface. In this study, a 3-D simulation model is built, where the wettability alteration of chalk is linked to the amount of sulfate adsorption in an anion exchange process. By using the simulation software IORCoreSim, the dynamical shift from a neutral wetting system towards a more water-wet system is illustrated, and the simulated oil recoveries are matched towards laboratory experiments executed by Puntervold *et al.* (2015).

The results showed that the anion exchange model can capture a wettability alteration due to sulfate adsorption in carbonate reservoirs. The model can predict the main oil recovery trends of the laboratory experiments (Puntervold *et al.*, 2015), but is sensitive to important parameters as the temperature of the system and the concentration of Ca^{2+}. It has been concluded that the anion exchange model is not adequate to thoroughly capture the complexity of these systems, however, the model can be used as a basis for further investigations.

Table of contents

List of Figures

List of Tables

Symbols and Abbreviations

NFR	Naturally Fractured Reservoir
OOIP	Original Oil in Place
SI	Spontaneous Imbibition
EOR	Enhanced Oil Recovery
S_w	Water saturation
S_{wi}	Initial water saturation
S_{or}	Residual oil saturation
SW	Sea Water
WA	Wettability Alteration
SK	Stevns Klint chalk
AN	Acid Number (mg KOH/g)
P_c	Capillary pressure
k_{rj}	Relative permeability of phase j
USBM	U.S Bureau of Mines
SWXNa	Modified seawater with "X" times the NaCl concentration of ordinary SW
SW0NaXS	Modified seawater depleted in NaCl with "X" times the SO_4^{2-} concentration of ordinary SW

Chapter 1

1 Introduction

1.1 Background

Enhanced oil recovery by spontaneous imbibition (SI) of a wetting liquid into porous media is of great importance in naturally fractured reservoirs. Several studies have been carried out by researchers to improve the understanding of the physical processes behind the SI mechanism. Most of the SI experiments are conducted under a counter-current flow assumption, where the wetting fluid imbibes into a porous medium and displace the non-wetting phase by the action of capillary pressure.

According to Xie *et al.* (2004), SI is only possible when a large enough portion of the pore surfaces are adequately water-wet in order for the water to imbibe into the matrix while oil are pushed along the fractures towards the producer. However, most of the fractured carbonate reservoirs are oil-wet and will hold more strongly onto the oil compared to a water-wet rock. Consequently, the wettability of the rock need to be altered to get an increased EOR effect.

Multiple imbibition experiments are found in the literature where the composition of the imbibing brine is varied. In (Zhang & Austad, 2006; Zhang *et al.*, 2007), several tests were utilized on carbonate cores during SI of seawater brines with modified composition. The results showed an increase in oil recovery, which may be explained by a wettability alteration of the mineral surface. By changing the concentration of naturally existing ions in seawater, the mineral surface is altered towards a more water-wet state and a greater amount of oil is displaced by the injected water. Previous studies (Fathi *et al.*, 2011b; Puntervold *et al.*, 2015) have also shown that the EOR effect of seawater can be even smarter by removing Na^+ and Cl^- ions and increase the SO_4^{2-} concentration of the imbibing water.

The SI process in fractured carbonates involves complex interactions between the imbibing Smart water, crude oil, formation water and the rock surface. Although several core-scale laboratory studies have been executed, it is necessary to implement a good simulation and numerical analysis due to the uncertainty and complexity of these systems.

Yu *et al.* (2009) developed a numerical one-dimensional model describing the SI process of seawater. The model included adsorption of SO_4^{2-} as well as molecular diffusion, capillary- and gravitational forces. The results indicated that the capillary pressure curve moved from an oil-wet system towards a more water-wet system and was proportional to a wettability alternating component.

A similar model was proposed by Evje and Hiorth (2011), which was based on the well-known Buckley-Leverett equation for two-phase SI. The water-saturation equation was connected to a range of reaction-diffusion (RD) equations to illustrate how changes in the wetting state of a chalk core are related to water-rock chemistry. The model was able to capture the main trends of the matched experimental results, particularly the dependency of the brine composition on enhanced oil recovery.

Rangel-German and Kovscek (2002) proposed an experimental equipment that was able to measure the imbibition rate in fracture and matrix blocks. They also presented an analytical solution for the flow of water into the matrix-fracture system by extending a one-dimensional solution for imbibition. Their findings showed that the recovery of oil was linear with time initially, becoming linear with the square root of time later. The results were consistent with the behavior of previous experiments conducted.

Qiao *et al.* (2015) further established a thorough multicomponent and multiphase reactive transport model that accounts for wettability alteration in carbonates. The model outlines the geochemical interactions in a Smart water system, specifically among the carboxylic groups, sulfate, cations and solid surface. The results showed that the oil production was proportional to the concentration of SO_4^{2-}, which are consistent with previous studies.

Although Smart water injection has shown significant promise in core experiments and numerical analysis, modelling of the EOR mechanisms are lacking. ECLIPSE is a well-known simulation software used in the industry worldwide, with the ability to propose the exploitation of a reservoir and testing different production scenarios for oil recovery optimization. However, it may be difficult to implement the complex geochemical interactions involved in a Smart water injection process. Nonetheless, the simulation tool IORCoreSim have a more advanced

chemistry and can be used to model the interactions among different species and phases in chemically tuned injection water. IORCoreSim is also capable of providing improved interpretations of laboratory experiments, as well as reducing the uncertainty of field implementations.

1.2 Objective

The main objective of this thesis is to test whether an anion exchange model can be coupled to wettability alteration of carbonate reservoirs. The simulation software IORCoreSim is used to capture the behavior of the Smart water spontaneous imbibition experiments conducted by Puntervold *et al.* (2015) represented in ***Figure 1.1***. Outcrop Stevns Klint chalk (SK) was used as the porous medium, originating from nearby Copenhagen, Denmark. The petrophysical properties and the matrix material are comparable to the chalk oil reservoir Valhall, which is situated in the North Sea.

A 3-D simulation model is built based on the experimental data, where wettability alteration towards a more water-wet system is linked to the amount of SO_4^{2-} adsorbed on the chalk surface. The model aims to capture recovery profiles where the imbibing brine is gradually depleted in NaCl and spiked with 0-4 times the SO_4^{2-} concentration in seawater. Estimated recovery profiles are matched towards experimental data and discussed in terms of the suggested mechanisms of Smart water SI. Possible limitations or shortcomings of the model will be examined, especially the diffusion velocity of ions, anion exchange capacity, changes in temperature, oil chemistry and the impact of modifying the Ca^{2+} concentration. At last, potential improvements of the anion exchange model will be proposed and discussed.

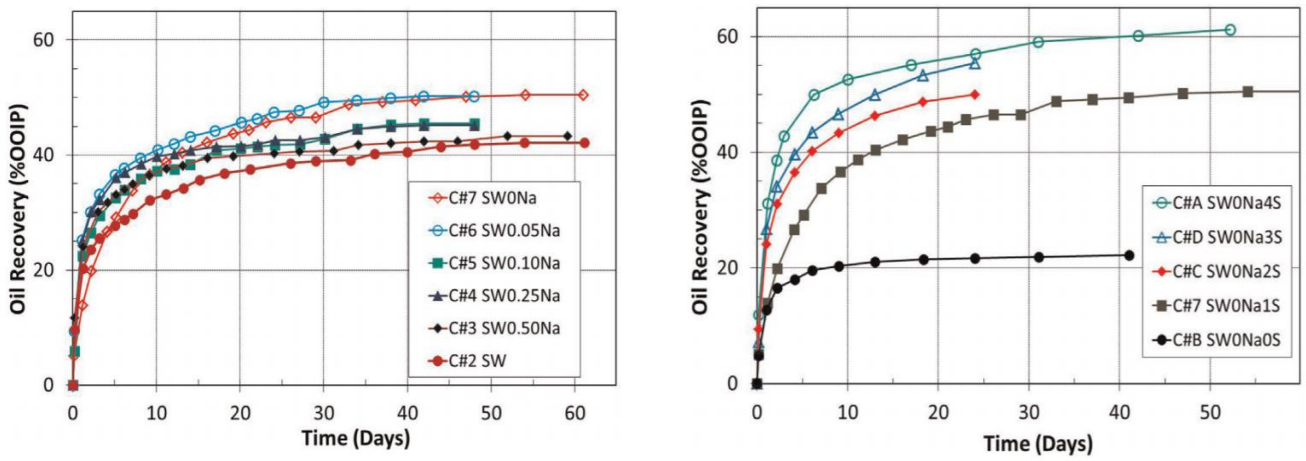

Figure 1.1 - *Oil Recovery for various Smart water SI experiments retrieved from Puntervold et al. (2015)*

Chapter 2

2 Fundamentals

2.1 Oil Recovery in Naturally Fractured Reservoirs

A large proportion of the worlds petroleum reserves are naturally fractured reservoirs (NFR). Natural fractures are caused by stresses in the formation due to tectonic forces such as faults and folds. In carbonate reservoirs, the formation consists of matrix blocks with relatively low permeability, which are disconnected from a dense fracture network. As follows, naturally fractured carbonate reservoirs may be challenging to produce.

According to Green and Willhite (1998), oil production from a reservoir can be divided into the following stages; primary recovery, secondary recovery and tertiary recovery. Primary production describes the first stage where oil displacement is driven by the energy initially stored in the reservoir. The main driving forces are gravity drainage, rock and fluid expansion, water drive, solution gas drive and gas cap drive. Generally, the recovery factor for primary production is very low and covers around 5-20 % of the original oil in place (OOIP).

Secondary oil recovery processes are usually implemented where the primary depletion reduces its driving force. Traditionally, external energies must be applied to increase oil recovery. These processes include injection of gas into the gas cap and/or injection of water into the aquifer to prevent a rapid pressure reduction and support the injection drive mechanism in the reservoir. NFRs are normally divided into fracture and matrix systems, where fluids in the fracture have the potential to flow more easily compared to fluids stored in the matrix. When water is injected in a secondary recovery process, it will follow the high permeable fracture network with the lowest flow resistance. Correspondingly, conventional waterflooding is unfavorable since the injected water will bypass any trapped oil inside the lower permeable blocks.

Tertiary recovery methods are almost synonymous with the Enhanced Oil Recovery (EOR) classification. EOR aims to recover the entrapped oil by primarily inject chemicals, thermal energy or gases to improve the sweep efficiency and extend the lifetime of a reservoir. The most common EOR processes are listed in ***Table 2.1***.

Table 2.1 *- Classification of EOR processes taken from Thomas (2008)*

Thermal	Hot Water Steam In-Situ Combustion Electrical Heating
Miscible	Slug Process Enriched Gas Drive Vaporizing Gas Drive CO_2 Miscible N_2 Miscible Alcohol
Chemical	Polymer Surfactant Alkaline Micellar ASP Emulsion

At the end of the 19th century, another EOR method was proposed by Morrow (1990) , namely to alter the wettability of the reservoir by changing the ionic composition of the injected water. Most fractured carbonate reservoirs have a significant amount of oil in place (OOIP), which results in a great interest for improving oil recovery. One of the main EOR mechanisms in such reservoirs is wettability alteration by SI of seawater/modified seawater, which will be a central area of interest in this thesis. ***Table 2.2*** feature the fundamental processes within this EOR method.

Table 2.2 *- EOR processes by water-based wettability alteration retrieved from Thomas (2008)*

Wettability Alteration by SI	Smart Water Low salinity (Sandstone) Seawater/modified Seawater (Carbonate)

2.2 Spontaneous Imbibition in NFRs

When water is injected into NFRs to optimize recovery, oil is displaced from the higher permeable zones during advective flow and the fractures are saturated with water. The advective flow of water and oil will only follow the paths of the fractures, while capillary driven flow is able to follow the parts of the matrix that stores most of the oil. Thus, if the capillary forces are efficiently high, water will imbibe into the less permeable parts of the matrix in a SI process and redistribute water and oil. Consequently, capillary forces are of great importance in NFRs.

SI arise where the wetting phase spontaneously displaces the non-wetting phase in a porous medium. The process is often divided into two types of flow, namely co-current and counter-current imbibition. During a co-current flow, oil and water will move into the fracture volume in the same direction, while oil is expelled from the rock. In core analysis experiments, SI will in many cases be a counter-current imbibition process, where water and oil flow in the opposite directions. When a core sample is placed in a container with a surrounding water-bath, the water will automatically imbibe into the rock without any applied pressure. The counter-current SI process is driven by the capillary pressure (P_c), where the smallest pores are displaced first due a higher P_c. Afterwards, the water extends to the larger pores and oil is expelled from the core. The process is visualized in ***Figure 2.1***.

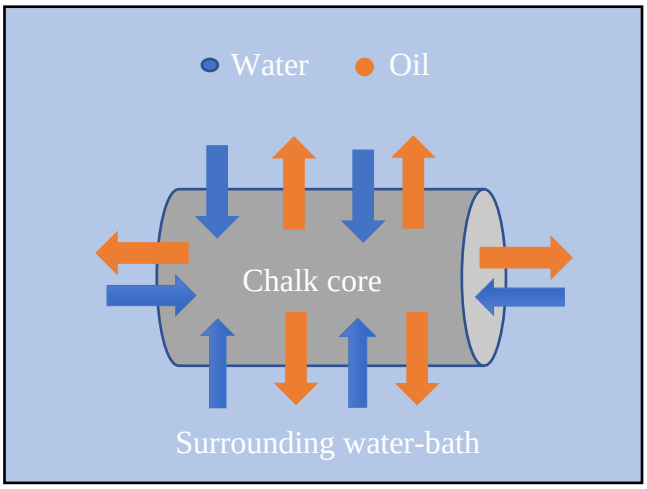

Figure 2.1 *- Schematic overview of a counter-current imbibition process in a chalk core with all faces open for flow*

2.3 Wettability

Even though SI of water is regarded as one of the most efficient methods to retrieve oil from fractured reservoirs, the process is strongly dependent on the matrix wettability. It is believed that the wettability of a reservoir gives information about the potential of oil recovery by spontaneous and forced imbibition. Accordingly, researches have spent a large amount of time understanding the relation between EOR and wettability. In fractured reservoirs, multiple interactions between the rock/brine/crude oil makes the system remarkably complex. Each phase contains several individual components, which can influence the wetting of the reservoir.

2.3.1 Wettability definition

When two non-miscible liquids are present at the same time near a surface of a solid, there exists a cohesive force between the liquid molecules and the molecules at the surface. As represented by Anderson (1996), wettability can be defined as *"the tendency of one fluid to spread on or adhere to a solid surface in the presence of other immiscible fluids."* The fluid with the highest affinity to the solid surface is called the wetting phase, whereas the other fluid is called the non-wetting phase. Another closely related definition is given by Jerauld and Rathmell (1997), who states that *"wettability is defined as the tendency of one fluid of a fluid pair to coat the surface of a solid spontaneously."*

2.3.2 Wettability classification

Wettability is both a continuous and complex parameter that controls the flow, distribution and location of the fluids in a reservoir. Nevertheless, it is often grouped into three categories; oil-wet, water-wet and intermediate-wet (neutral wet).

In an oil-wet reservoir, the oil will occupy the smallest pores in the matrix and contact most of the rock surface, while water is situated in the middle of the pore volume. Similarly, if the rock is water-wet, most of the rock surface is in contact with water, and water will occupy the smallest pores. An intermediate-wet/neutral-wet system will show little to no preference between the two fluids.

Previous work (Morrow, 1990) has shown that researchers originally believed that oil reservoirs had a strongly water-wet surface, and that the connate water would shelter the entering crude oil from covering the rock surface. Nonetheless, laboratory work done by Treiber and Owens (1972) indicated that the majority of the 55 cores tested were in the oil-wet range, especially the carbonate reservoirs. They believed that the reason was that some of the constituents in the crude oil had the possibility to alter the wetting from an original water-wet system towards an oil-wet system, despite the protecting water shelter.

It is now generally accepted (Salathiel, 1973) that some reservoirs have become oil-wet over time, and those reservoirs are classified as being mixed-wet. In such systems, the grain contacts and the smaller pores would preferentially be water-wet, while the larger pore surfaces are strongly oil-wet. The oil will flow as a film if the oil-wet paths are continuous, and consequently only a minor amount of oil would be trapped in the smaller pores due to capillary forces. Mixed-wet systems can also occur due to heterogeneities and variations in the chemistry and composition of the reservoir rock. This wetting state is often referred to as fractional-wet, where a portion of the rock is strongly oil-wet, and the other portion is strongly water-wet. ***Figure 2.2*** is taken from Abdallah et al. (2007) and illustrates the initial fluid distribution in a water-wet, mixed-wet and oil-wet system respectively.

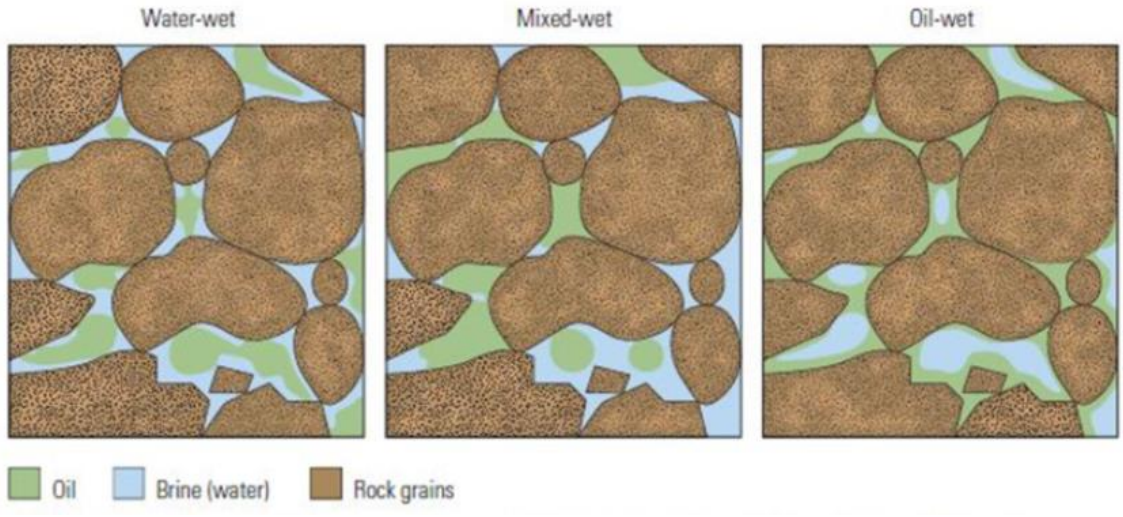

Figure 2.2 *- Initial fluid distribution of a reservoir rock in a water-wet, mixed-wet and oil-wet system respectively. Retrieved from (Abdallah et al., 2007)*

2.3.3 Wettability measurements

Several methods exist for determining the wetting properties of a porous medium, and they are usually categorized into quantitative and qualitative methods. Quantitative methods include contact angle measurement, Amott-Harvey Index and U.S Bureau of Mines (USBM). All these methods are considered as being direct tests of the wettability. Furthermore, qualitative methods are indirect measurements including microscope examination, chromatographic wettability test, imbibition rates and capillary pressure curves. The USBM method together with the chromatographic wettability test will be outlined in more detail below.

2.3.3.1 U.S Bureau of Mines (USBM)

According to Donaldson *et al.* (1969), the USBM method is a quantitative approach for measuring the average wettability of a core sample using capillary pressure curves. The core with irreducible water saturation is rotated in a water filled tube by a centrifuge. By increasing the speed stepwise, the sample eventually reaches residual oil saturation. Afterwards, the sample is placed into an oil-filed tube for another sequence of measurements. The USBM index (WI_{USBM}) is related to the work required for the wetting phase to displace the non-wetting phase, which corresponds to the area behind the capillary pressure curves as indicated in ***Figure 2.3***.

$$WI_{USBM} = \log\left(\frac{A_1}{A_2}\right) \qquad \text{(eq. 2.1)}$$

where A_1 is the area under the curve where oil displaces water, whereas A_2 is the area under the curve where water displaces oil.

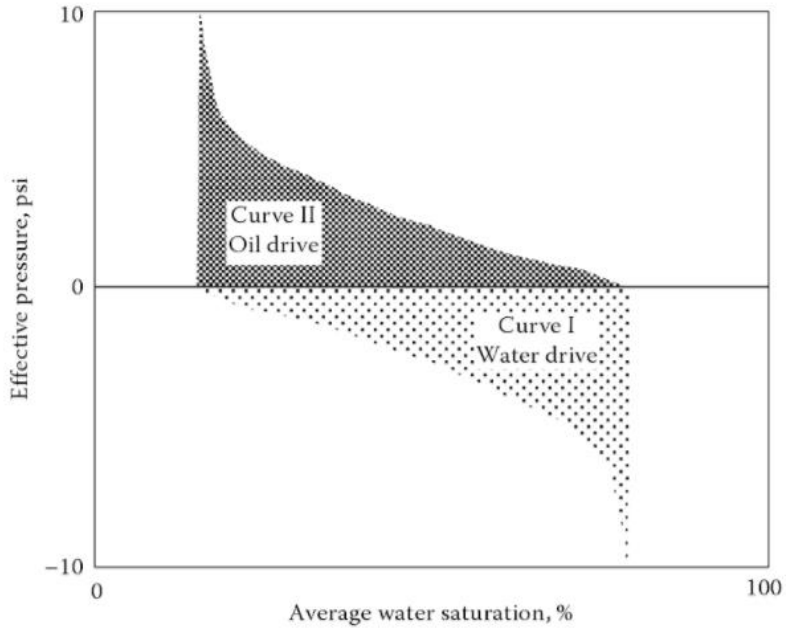

Figure 2.3– *Plot of effective pressure vs. average water saturation where oil displaces water (Curve II) and where water displaces oil (Curve I) taken from Dandekar (2013)*

According to Abdallah *et al.* (2007), the USBM index varies between ∞^- (strongly oil-wetting) and ∞^+ (strongly water-wetting), although most of the measurements extends from -1 to +1. The method is relatively fast and quite sensitive close to neutral wettability. However, the test can only be done on plug-size samples, and it cannot determine whether the system has mixed or fractional wettability.

2.3.3.2 Chromatographic Wettability test

The chromatographic wettability test was developed by Strand *et al.* (2006b), and is based on a chromatographic separation of two water-soluble components during a flooding process in carbonates, namely SCN^- (non-adsorbing tracer) and SO_4^{2-} (potential determining ion). Since carbonates have a positively charged surface, the sulfate ions will adsorb onto the water-wet sites. Thus, the wetting index parameter is assumed to represent the fraction of the carbonate surface covered by water, where the amount of adsorption depends on the wetting state of the rock. The process is visualized in ***Figure 2.4*** below.

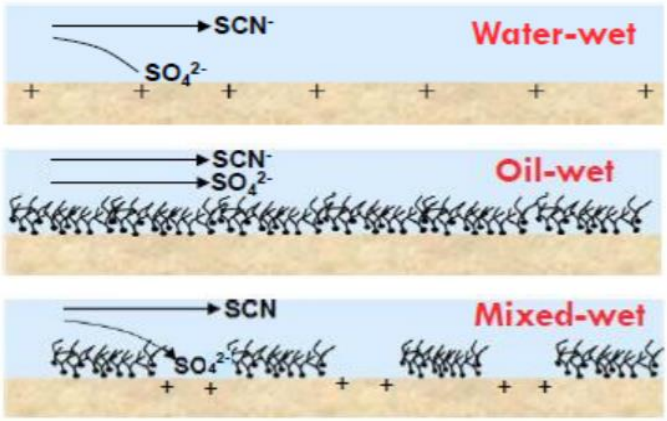

Figure 2.4 *- Adsorption of SO_4^{2-} on a water-wet, oil-wet and mixed-wet carbonate surface retrieved from Shariatpanahi (2012)*

By flooding a core at residual oil saturation (S_{or}), it is possible to measure the area between the effluent profiles for SCN^- and SO_4^{2-}. Consequently, the area will be proportional to the amount of water that covers the carbonate surface, A_{wett}. The water index is defined as the ratio between A_{wett} and a corresponding area in a completely water-wet reference core, A_{ref}.

$$WI = \frac{A_{wett}}{A_{ref}} \qquad \text{(eq. 2.2)}$$

WI varies between 0 and 1, where 0 represents a completely oil-wet system, and 1 indicates a perfectly water-wet system. ***Figure 2.5*** is based on the studies of Strand *et al.* (2006b) and gives a schematic overview of the effluent profiles of SCN^- and SO_4^{2-}, in addition to the area used in calculating the wetting index.

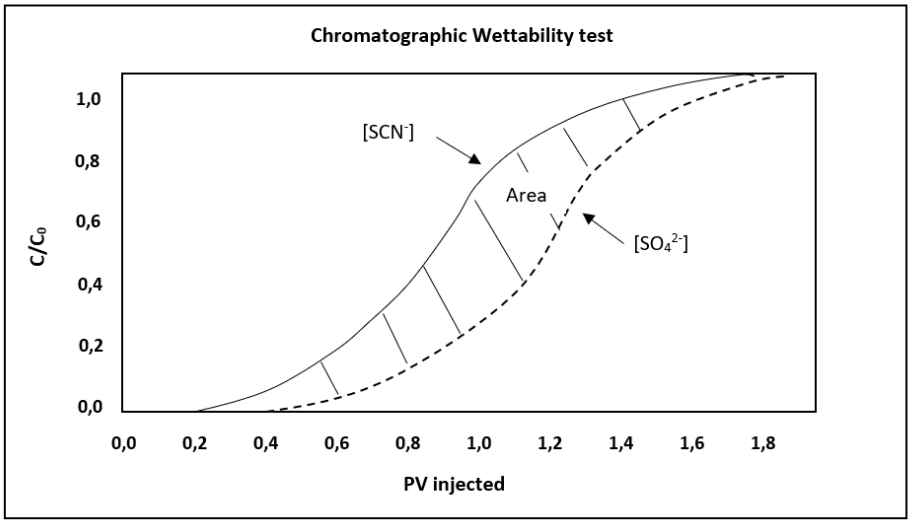

Figure 2.5 *– Schematic overview of the chromatographic wettability test and the separation between effluent profiles of SCN^- and SO_4^{2-} based on the studies of Strand et al. (2006b)*

2.4 Relative permeability and Capillary Pressure

In carbonate reservoirs, the initial wetting has an apparent impact on important reservoir parameters, such as the relative permeability of oil and water, the capillary pressure and the distribution of fluids in the reservoir. The magnitude of the capillary pressure is the driving force in a SI process, while the mobilities of oil and water controls the rate of the process. Consequently, the total oil recovery is highly dependent on the interactions between the fluids at the surface of the rock as well as inside the pores.

2.4.1 Relative Permeability Curve

The permeability of a reservoir rock is a measure of the ability the porous medium has to transport fluids through the pores. Large continuous pore openings are associated with high permeability, while small, contiguous pores are related to low permeability. Permeability is also a tensor, where the size often varies in different directions. Thus, the degree of anisotropy is of great importance when predicting flow patterns and for optimizing

production strategy. Darcy's law for a linear horizontal flow of an incompressible liquid through a porous medium can be written as follows;

$$Q = -\frac{AK}{\mu}\left(\frac{\partial P}{\partial x}\right) \quad \text{(eq. 2.3)}$$

where Q is the flowrate of the formation, A is the cross-sectional area, K is the absolute permeability, μ is the viscosity of the fluid and $\frac{\partial P}{\partial x}$ is the pressure change per unit length of the formation.

Nonetheless, an oil reservoir is often saturated of more than just one phase. Consequently, there will be less space for the fluid to flow within the porous medium. The relative permeability (k_{rj}) is thus defined as the effective permeability a fluid experience, divided by the absolute permeability of the porous medium;

$$k_{rj} = \frac{k_{eff}}{K} \quad \text{(eq. 2.4)}$$

The wetting fluid in a porous media will generally occupy the smallest pores and be distributed as a thin film in the larger pores. The non-wetting fluid will in comparison be situated in the center of the larger pores, resulting in a higher fluid relative permeability. This is clearly visualized in ***Figure 2.6*** taken from Anderson (1987b), where k_{rw} is higher in the oil-wet system compared to the water-wet system. This phenomenon occurs because the oil in the oil-wet system tends to move between the less permeable pores, while water flow more easily in the larger pores. Furthermore, at low water saturations, some of the water will get trapped in the larger pores, causing a blocking of the pore throats, resulting in a lower permeability of oil.

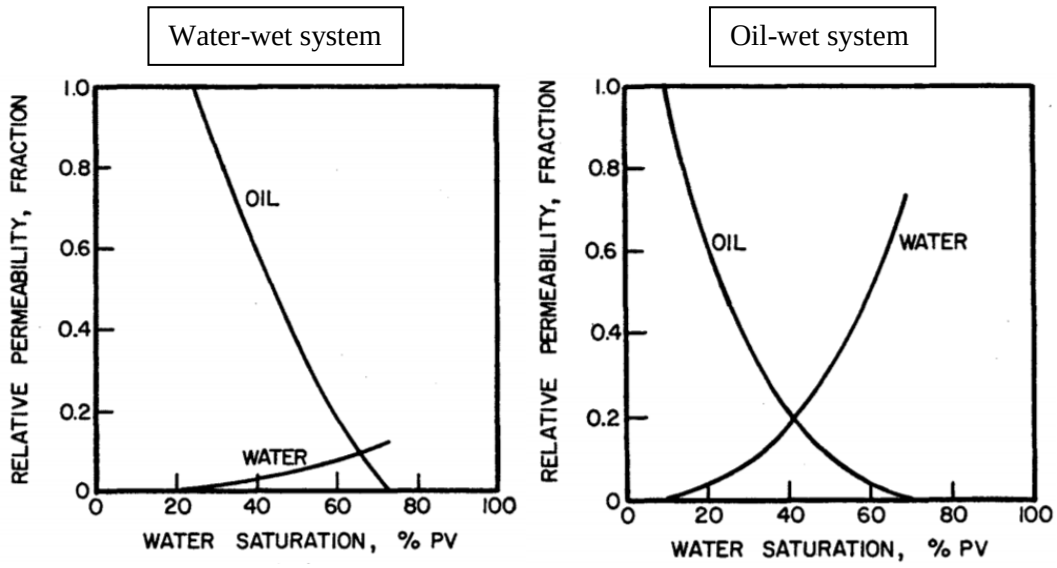

Figure 2.6 *- Relative permeability curves in a water-wet system (left) and in an oil-wet system (right) taken from Anderson (1987b)*

2.4.2 Capillary Pressure Curve

Capillarity is the physical phenomenon that causes a wetting liquid to enter thin capillary tubes. The effect is due to surface tension, which occurs on the interface among two liquids, and is defined as:

$$\sigma = \frac{dW}{dA} \qquad \text{(eq. 2.5)}$$

where dW is the work required to increase the fluids surface with an area dA.

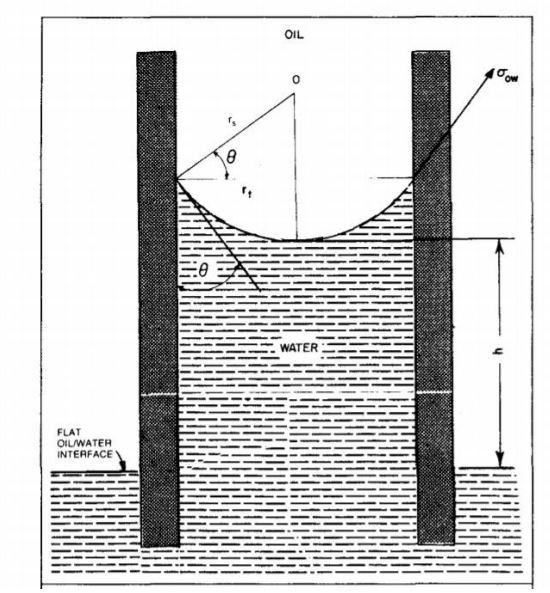

Figure 2.7 *- Oil/water interface in a capillary tube taken from Anderson (1987a)*

Figure 2.7 illustrates the interfacial tension between oil and water in a capillary tube. The oil droplet has a radii *R*, which is decided by the surface tension σ, water pressure P_w and oil pressure P_o. The surface tension tries to minimize the droplets surface, which results in a force acting inwards. The work required to increase the radii of an oil droplet with area *dR* thus becomes;

$$dW = F \cdot dR = (P_o - P_w) \cdot 4\pi \cdot R^2 \cdot dR \qquad \text{(eq. 2.6)}$$

The area of the droplet surface is $A=4\pi R^2$. An increase of the area due to an increase in the radii is then $dA=8\pi RdR$. It follows from *eq. 2.5* that the surface tension can thus described as;

$$\sigma = \frac{dW}{dA} = \frac{(P_o - P_w) \cdot 4\pi \cdot R^2 \cdot dR}{8\pi \cdot R \cdot dR} = \frac{(P_o - P_w) \cdot R}{2} \qquad \text{(eq. 2.7)}$$

If the defining surface between oil and water is not spherical, two different curvature radii are needed, namely R_1 and R_2. The new expression is called the *Laplace equation*:

$$P_c = P_o - P_w = \sigma \cdot \left(\frac{1}{R_1} + \frac{1}{R_2}\right) \qquad \text{(eq. 2.8)}$$

As illustrated in ***Figure 2.7***, the fluid saturation is strongly related to the curvature radii between oil and water. Consequently, the capillary pressure depends on the fluids that wets the porous medium. The different stages in a capillary pressure curve is shown below in ***Figure 2.8***.

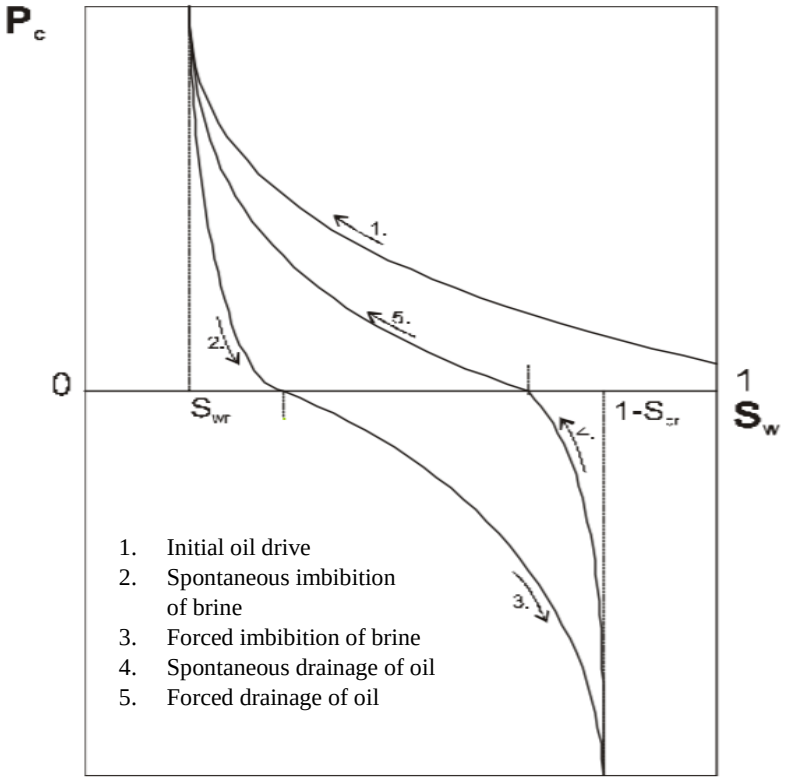

Figure 2.8 *- Capillary pressure curves vs. water saturation retrieved from Høgnesen (2005)*

At the start of the initial oil drive curve (labeled 1) in ***Figure 2.8***, the core is initially filled with water. Before oil can enter the system, an entry pressure must be exceeded. As the capillary pressure increases, the water saturation decreases, and more oil can enter the core. As the externally applied capillary pressure reaches a sufficiently high value, the wetting phase will be separated from the bulk wetting phase. Thus, the continuity of the water phase is lost, and the system has reached an irreducible water saturation. Furthermore, after the primary drainage curve has been measured, the capillary pressure is steadily decreased to zero in a SI process (labeled 2). At $P_c = 0$, some of the oil will still be connected to the rock surface, therefore, the residual oil saturation will not be the irreducible oil saturation. For a more water-wet system, Pc = 0 at a higher water saturation. Consequently, the capillary pressure determines how much

oil that can be recovered. Lastly, the capillary pressure is lowered from zero to a negative value, where a forced imbibition of brine takes place (labeled 3). As the capillary pressure is negative, $P_w > P_o$ and water is forced into the rock until the water saturation reaches $1\text{-}S_{or}$. Curve number 4 represents spontaneous drainage of oil, which happens if P_w is slowly reduced. In this process, the capillary pressure increases from a negative value to zero and will reach a water saturation which is higher than during SI of brine. The water saturation can also be reduced further by applying forced drainage of oil (curve 5), which will finally arrive at the start of the SI curve (Anderson, 1987a).

2.4.2.1 Wettability Effects on the Capillary Pressure curve

The P_c - curve will be different depending on the wettability of the system. In a more water-wet reservoir, S_{or} is reduced since the oil is more mobile and situated in the middle of the pores. Correspondingly, the water saturation increases where the curve crosses zero capillary pressure. Zhou *et al.* (2000) examined this process by executing SI and waterflood experiments on several Berea sandstone cores with different S_{wi} and initial wetting. It should be mentioned that the same behavior has also been observed in chalk cores. Behbahani and Blunt (2005) interpreted the experiments numerically and further investigated how the aging time of the reservoir rock impacted the capillary pressure curve. In this context, aging time is referring to a wetting state, where a non-aged core represents a strongly water-wet system. The results from the study showed that as the aging time increases, corresponding to more of the pore space being oil-wet, P_c reduces to a lower value and a higher fraction of the curve is situated below zero. Since recovery by SI is controlled by the fraction of the P_c – curve situated above zero, a decrease in recovery is expected as more of the pore space are oil-wet. This is because SI will be limited to a small saturation range with a low S_w, due to poor water connectivity through the pore network. Consequently, the water relative permeability is remarkably low, giving recovery rates 10^1 – 10^3 times smaller compared to a water-wet rock. Aging time of the cores investigated, and their wetting states are shown in ***Figure 2.9***. Note that in a strongly water-wet rock, all the mobile oil can be produced in a SI process.

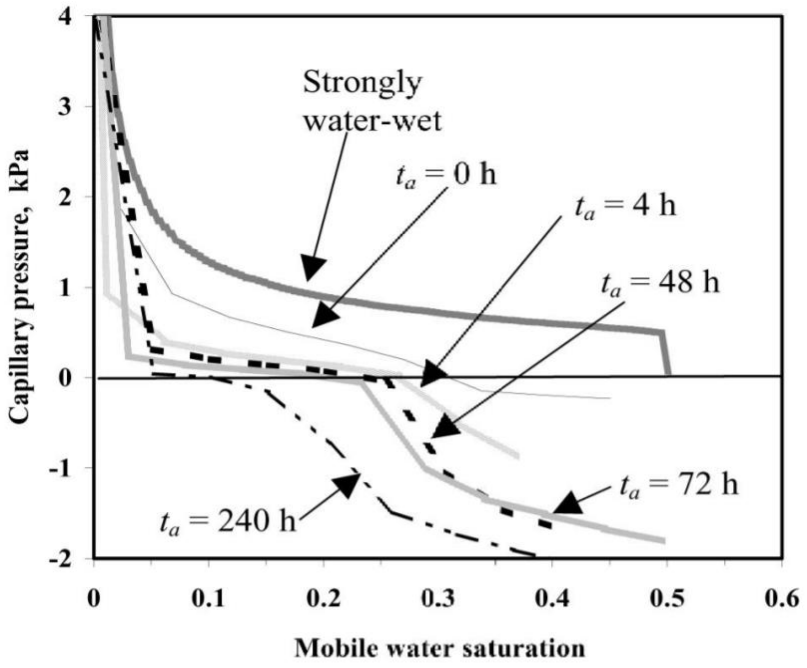

Figure 2.9 *- Capillary pressures for different aging times (t_a) corresponding to different wettability states, retrieved from Behbahani and Blunt (2005)*

Chapter 3

3 Smart Water as an EOR mechanism in Carbonates

3.1 Wetting properties in Carbonates

It is assumed that almost all carbonate reservoirs were initially water-wet, and that the carbonate surface was in equilibrium with the surrounding formation water. The formation water contains Ca^{2+}, resulting in a positively charged surface with pH < 9. When oil migrated into the reservoir and displaced water, the interface between the water-wet rock surface and the oil became negatively charged. This is due to partial separation of the carboxylic acid groups (-COOH) in the crude oil, which results in negatively charged carboxylates ($-COO^-$). Consequently, the carboxylates have the possibility to adsorb onto the carbonate surface making it less water-wet. Previous studies (Puntervold *et al.*, 2007) have shown that the degree of water-wetness is associated with the acid number (AN), which is an estimate of acidic material present in the crude oil. A higher AN indicates that more of the carboxylates can adsorb onto the carbonate surface and reduce the initial water-wetness of the reservoir.

3.2 Mechanisms of Smart Water injection in Carbonates

Modified seawater has been regarded as a "smart" EOR fluid in carbonate reservoirs due to its capability of increasing the water-wetness of the rock surface. It is suggested that the wettability alteration is due to the interaction among the rock surface and the potential determining ions Mg^{2+}, Ca^{2+} and SO_4^{2-} present in seawater.

The Smart water mechanism implies that SO_4^{2-} adsorbs onto the positively charged water-wet sites on the carbonate surface and reduces the net surface charge. Due to less electrostatic repulsion, the concentration of Ca^{2+} close to the surface increases and calcium complexes with carboxylates. Subsequently, some of the organic materials are released from the surface and can contribute to a higher oil recovery. According to Strand and Puntervold (2017), sulfate acts as the catalyst in a Smart water SI process, but the adsorption is highly dependent on the amount of calcium ions in the system.

Mg^{2+} is a strongly hydrated ion in water, meaning it has a small reactivity at lower temperatures. However, at higher temperatures, the magnesium ions get remarkably reactive due to the splitting of hydrogen bonds. Accordingly, Mg^{2+} have the possibility to substitute Ca^{2+} at the carbonate surface and hence displace calcium connected to the carboxylates. Correspondingly, the degree of substitution increases with temperature. The reaction is illustrated by the following equilibrium:

$$CaCO_3\,(s) + Mg^{2+} \rightleftharpoons MgCO_3(s) + Ca^{2+} \qquad \text{(eq. 3.1)}$$

Nevertheless, since the experiments investigated in this thesis are conducted at a relatively low temperature (90 ℃), Mg^{2+} is assumed to have a minor contribution to the wettability alteration process. Correspondingly, only the effect of Ca^{2+} and SO_4^{2-} will be tested in the simulations.

Figure 3.1 is taken from Zhang *et al.* (2007) and highlights the suggested mechanisms for wettability alteration by smart water injection. *(A)* shows the mechanism where SO_4^{2-} adsorbs and lower the surface charge where Ca^{2+} reacts with the adsorbed carboxylic group and release it from the surface. *(B)* emphasize the substitution reaction of Ca^{2+} with Mg^{2+} at higher temperatures.

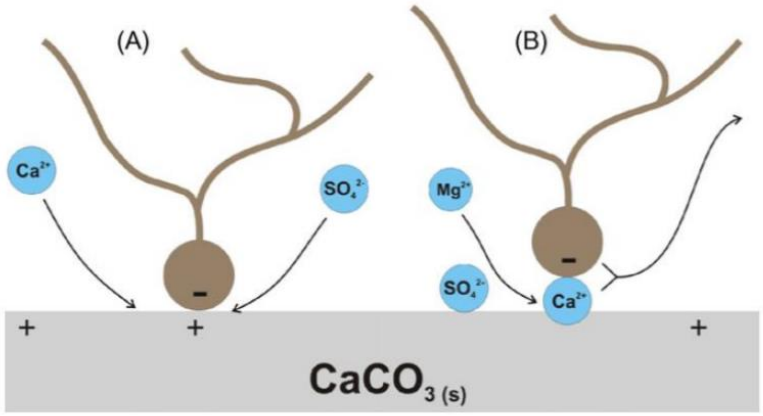

Figure 3.1 *- Suggested mechanisms for a wettability alteration in CaCO3 (s) taken from Zhang et al. (2007)*

3.3 Electrical double layer

A charged surface will have the potential to affect the distribution of ions in the surrounding area of a polar medium. Ions with the opposite charge of the surface will be attracted, while those with equal charge will be rejected. This, together with the thermal motion of the ions, forms an electrical double layer.

The double layer can be divided into two parts according to Sterns theory; an immobile and a mobile part as visualized in ***Figure 3.2*** taken from Du *et al.* (2015). The immobile part is situated closest to the surface and is referred to as the Stern Layer. This layer consists of adsorbed ions and is only 1-2 molecular diameters thick. The transition between the immobile and the mobile part of the double layer is called the shear plane. The mobile part consists of a diffusive layer, where the ions are not bounded to the surface.

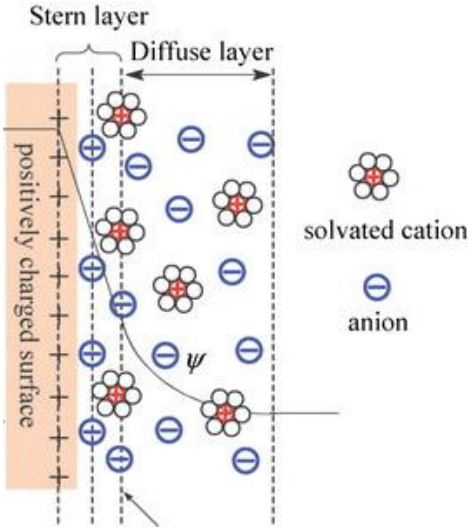

Figure 3.2 *- Schematic figure of the different parts of the electrical double layer taken from Du et al. (2015)*

It is generally believed that when there is an increase in the electrolyte concentration, the diffusive part of the electrical double layer will be compressed. This means that a reduction in the salt content around the surface can give a wider double layer. Correspondingly, the salt density near the surface is reduced, and the access of Ca^{2+}, Mg^{2+} and SO_4^{2-} to the surface increases. Consequently, a reduction in the electrolyte concentration of the imbibing brine may give a higher oil recovery.

3.4 Chemical reactions

Since chalk is composed of $CaCO_3$(s), SI of Smart water may lead to several chemical reactions. Only some of the reactions are discussed in this thesis, like dissolution/precipitation, water complexations and ion exchange. Special emphasis has been on reactions including the potential determining ions Ca^{2+}, Mg^{2+} and SO_4^{2-}, but other species present in SW and FW will follow the same equations. Below are some of the chemical reactions that will be discussed more thoroughly in the discussion part of the thesis. Note that Z^+ represent the positive and X^- the negative surface sites in the ion exchange reactions respectively.

Dissolution/precipitation

$$CaCO_3(s) \rightleftharpoons Ca^{2+} + CO_3^{2-}$$ (eq. 3.2)

$$Ca^{2+} + SO_4^{2-} \rightleftharpoons CaSO_4(s)$$ (eq. 3.3)

Water complexations

$$Na^{+} + SO_4^{2-} \rightleftharpoons NaSO_4^{-}$$ (eq. 3.4)

$$Ca^{2+} + Cl^{-} \rightleftharpoons CaCl^{+}$$ (eq. 3.5)

$$Mg^{2+} + Cl^{-} \rightleftharpoons MgCl^{+}$$ (eq. 3.6)

Ion exchange

$$XNa \rightleftharpoons Na^{+} + X^{-}$$ (eq. 3.7)

$$X2Ca \rightleftharpoons 2X^{-} + Ca^{2+}$$ (eq. 3.8)

$$X2Mg \rightleftharpoons 2X^{-} + Mg^{2+}$$ (eq. 3.9)

$$XK \rightleftharpoons X^{-} + K^{+}$$ (eq. 3.10)

$$Z2SO_4 \rightleftharpoons SO_4^{2-} + 2Z^{+}$$ (eq. 3.11)

$$ZCl \rightleftharpoons Cl^{-} + Z^{+}$$ (eq. 3.12)

$$ZHCO_3 \rightleftharpoons HCO_3^{-} + Z^{+}$$ (eq. 3.13)

Chapter 4

4 Modelling the Smart Water SI process

4.1 Mathematical 3-D model based on Darcy's law

The fundamental equations to describe transport of two or more phases in a porous medium are differential equations that depict conservation of mass, Darcy law, and capillary pressure curves to relate the phase pressures. The following mathematical descriptions are based on part of the work done by Qiao *et al.* (2018). In the following we will take a closer look at a model for two immiscible and incompressible fluids in a porous medium. This model is used to find numerical solutions to the counter-current imbibition process. The contribution of gravity effects will be neglected since the vertical displacement of the fluids is small compared to the capillary forces. A 3-D model is necessary since the experiments are conducted on a cylindrical core, where the boundary conditions of the spontaneous imbibition process require a 3-D system. The 3-D transport equations for water and oil are given by:

$$\varphi \frac{\partial S_w}{\partial t} + \nabla \overrightarrow{u_w} = 0 \qquad \text{(eq. 4.1)}$$

$$\varphi \frac{\partial S_o}{\partial t} + \nabla \overrightarrow{u_o} = 0 \qquad \text{(eq. 4.2)}$$

where φ is porosity, S is saturation, u is the Darcy velocity and the subscripts o/w represents oil and water phases. Darcy velocity is defined as:

$$\overrightarrow{u_j} = -K\lambda_j \nabla P, \qquad \lambda_j = \frac{kr_j}{\mu_j} \ (j = w, o) \qquad \text{(eq. 4.3)}$$

where λ_j is the mobility of phase *j*, *K* is the tensor notation for absolute permeability and ∇P the pressure gradient of the system in x-, y- and z-direction respectively. Substituting the extended Darcy's law into *eq. 4.1* and *eq. 4.2* yields the following 3-D transport equations for water and oil:

$$\varphi \frac{\partial S_w}{\partial t} + \nabla \cdot (K_w \lambda_w \nabla P_w) = 0 \qquad \text{(eq. 4.4)}$$

$$\varphi \frac{\partial S_o}{\partial t} + \nabla \cdot (K_o \lambda_o \nabla P_o) = 0 \qquad \text{(eq. 4.5)}$$

The pressures and saturations are constrained by the following conditions:

$$P_c = P_o - P_w, \qquad S_w + S_o = 1 \qquad \text{(eq. 4.6)}$$

By adding the 3-D transport equations for water and oil, using the constraints introduced in *eq. 4.6*, it is reasonable to say that:

$$\partial_t (S_w + S_o) = -\nabla(\overrightarrow{u_w} + \overrightarrow{u_o}) = -\nabla \cdot \overrightarrow{u_T} = 0 \qquad \text{(eq. 4.7)}$$

The total Darcy velocity can be described using *eq. 4.3*, together with *eq. 4.6* and *eq. 4.7*:

$$\overrightarrow{u_T} = -K(\lambda_o \nabla P_o + \lambda_w \nabla P_w) \qquad \text{(eq. 4.8)}$$

Introducing the fractional flow of water and solving for ∇P_o gives:

$$f_w = \frac{\lambda_w}{\lambda_w + \lambda_o} = \frac{\frac{k_{rw}}{\mu_w}}{\frac{k_{rw}}{\mu_w} + \frac{k_{ro}}{\mu_o}} \qquad \text{(eq. 4.9)}$$

$$\nabla P_o = \frac{\lambda_o f_w}{\lambda_w} + f_w \nabla P_c - \frac{f_w u_T}{\lambda_w [K]} \qquad \text{(eq. 4.10)}$$

Since $\nabla P_w = \nabla P_o - \nabla P_c$, the equation above can be introduced to *eq. 4.8*. Correspondingly, the 3-D water-transport equation can be written on the following form:

$$\partial_t (S_w) + \nabla \cdot (\overrightarrow{u_T} f_w + K \lambda_o f_w \nabla P_c) = 0 \qquad \text{(eq. 4.11)}$$

Generally, k_{rj} and P_c - curves are functions of S_w and the ionic concentration of Smart water. This is because it is assumed that a WA component can change the functions by altering the wettability of the system. Therefore, it is more convenient to write the 3-D water-transport equation in the following form, where both λ_o and f_w depend on water saturation and chemistry:

$$\partial_t(S_w) + \nabla \cdot \left(\overrightarrow{u_T} f_w(S_w, F_m) + K\lambda_o(S_w, F_m)\, f_w(S_w, F_m)\, \nabla P_c(S_w, F_m) \right) = 0 \qquad \text{(eq. 4.12)}$$

where F_m represents an interpolation parameter between 0 and 1 that interpolates between two sets of saturation functions as the wettability of the system changes. Accordingly, F_m is directly coupled to a wettability alternating component, which will be outlined in more detail in *section 4.2*. *Eq. 4.12* must be given initial water distribution, as well as boundary conditions. Ω is defined as the domain of the core composed of calcite, while $\partial\Omega$ is the surface of the core.

Initial conditions

- $S_w(\Omega, t = 0) = S_{w,0}$ (eq. 4.13)

Boundary conditions

- $(x, y, x) \in \partial\Omega: S_w = 1$ (eq. 4.14)
- $P_c = 0 \in \partial\Omega$ (eq. 4.15)

The above equations describe a system containing water and oil. However, since the focus of this thesis is to model SI of modified seawater, additional equations need to be defined that illustrate the movement of different ions in the system. The transport equation for a general component *i* is defined below, where *i* is the different ions present in FW and the imbibing brines.

$$\partial_t(S_w C_i + \rho_i^s) = -\nabla \cdot (\overrightarrow{u_T} f_w C_i + K\lambda_o f_w C_i \nabla P_c) + \nabla \cdot (D_i S_w \nabla C_i) \qquad \text{(eq. 4.16)}$$

where C_i is the concentration of component *i*, ρ_i^s the adsorption of *i* at the surface and D_i the dispersion coefficient of *i*. The dispersion coefficient is described by an advective and a diffusive part:

$$D_i = \propto_{disp} u_w + D_{mol} \qquad \text{(eq. 4.17)}$$

where $\propto_{disp}$ is the dispersivity of the porous medium, u_w the water velocity and D_{mol} the molecular diffusion coefficient of the components.

The first term of *eq. 4.16* describes the advective flux, which is controlled by a bulk displacement of water containing a certain concentration of component *i*. The second term describe the water phase flow, which depend on the gradient in capillary pressure. Component *i* will flow together with water, but is also controlled by dispersion and diffusion according to the third term of the equation. Furthermore, the component *i* will be retained by adsorption (ρ_i^s), which is given in mol/L PV.

*Eq. 4.*16 must be given initial and boundary conditions. The initial conditions represent the composition of ions at the start, whereas the boundary conditions express the composition of the surrounding brine respectively.

Initial conditions

- $C_i\ (\Omega, t = 0) = \ C_{i,o}$ (referring to ***Table 5.3***) (eq. 4.18)

Boundary conditions

- $C_i\ (\partial\Omega, t) = \ C_i^{imb}$ (referring to ***Table 5.4*** and ***Table 5.5***) (eq. 4.19)

4.2 Anion exchange as a model for WA

According to Halling-Sorensen et. al (1993), ion exchange is a process where ions in a solution are exchanged for ions detached to the surface of a solid. Since calcite is composed of Ca^{2+} and CO_3^{2-}, these ions will represent the positive (Z^+) and negative surface sites (X^-) respectively. When Smart water spontaneously imbibes into the chalk core, SO_4^{2-} will adsorb onto the positive water-wet surface sites, whereas Ca^{2+} complexes with carboxylates and release the oil from the surface. Thus, it would be natural to use a model that can couple wettability alteration to the adsorption of SO_4^{2-} and co-adsorption of Ca^{2+}.

However, since IORCoreSim is still in the development phase, it only links wettability alteration to the concentration or adsorption of a single component. In this thesis, the wettability of chalk will be altered according to the amount of SO_4^{2-} adsorbed on the surface in an anion exchange process. Initially, all the ions in the formation water will compete against the positive

and negative surface sites. Since FW contains zero concentration of sulfate, ions adsorbed on the positive surface sites are exchanged with Cl^- and HCO_3^- referring to *eq. 3.12* and *eq. 3.13* respectively. When a brine containing sulfate is introduced to the system, SO_4^{2-} will also compete against the available Z^+ sites for adsorption referring to *eq. 3.11*, and an anion exchange process will take place.

Since sulfate is assumed to be the wettability alternating component, the system moves towards a more water-wet state as the amount of sulfate adsorption increases. The adsorbed amount of sulfate (ρ_{SO4}^s) is directly linked to an interpolation parameter (F_m), which interpolates between two sets of saturation functions. The first saturation function represents the initial wetting of the system, whereas the last saturation function defines a more water-wet system. It was decided to use the same relative permeability curves for the different wetting systems (explanation given in *section 6.3.1)*, so that the interpolation only occurs between the Pc-curves.

$$P_{c,interpolated} = Fm \cdot P_{c2}(S_w) + (1 - Fm) \cdot P_{c1}(S_w) \qquad \text{(eq. 4.20)}$$

where Pc_1 represents the first capillary pressure curve at a given S_w and P_{c2} the second capillary pressure curve at the same S_w. If there is no sulfate adsorption corresponding to zero ρ_{SO4}^s, F_m will be equal to zero and the saturation function representing the initial wetting will be used. Contrary, if sulfate occupies all the available positive surface sites for adsorption, F_m is equal to one and the saturation function representing a more water-wet system is used. This will be demonstrated in *section 6.5* where the adsorption isotherm of sulfate is outlined.

4.3 Correlations for the Saturation functions

The magnitude of the capillary pressure is the driving force in a SI process, while the permeabilities of oil and water determines the rate of the process. Since the objective of this thesis is to test if an anion exchange model can match experimental oil recoveries, the k_{rj} - and P_c – curves needs to be converted to tabulated values for corresponding water saturations. The correlations are presented in the following sections.

4.3.1 Correlation for Relative Permeability

Normally, when the permeabilities are measured in the laboratory, only endpoint values and values in between are used to generate relative permeability curves. Hence, analytical models are needed in a numerical study to include additional data-points between the measured values. In this thesis, modified Corey correlation from Standing (1974) was used to develop the relative permeability curves for water and oil.

$$k_{rw} = k_{rw}^{*} \cdot \left(\frac{S_w - S_{wi}}{1 - S_{or} - S_{wi}}\right)^{n_w} \quad \text{(eq. 4.21)}$$

$$k_{ro} = k_{ro}^{*} \cdot \left(\frac{S_o - S_{or}}{1 - S_{or} - S_{wi}}\right)^{n_o} \quad \text{(eq. 4.22)}$$

where k_{rw}^{*} is the endpoint relative permeability of water, k_{ro}^{*} the endpoint relative permeability of oil. Furthermore, n_w and n_o are constants used to modify the shape and curvature of the relative permeability curves for water and oil respectively. Corey exponents of oil and water for different wetting systems are presented in ***Table 4.1***.

Table 4.1 *- Corey exponents for different wetting systems retrieved from Stiles (2013)*

Wettability	N_o	N_w	$k_{rw\ end\text{-}point}$
Strongly Water-Wet	2 to 3	4 to 6	0.1 to 0.4
Mixed Wettability	3 to 5	2 to 4	0.5 to 0.9

4.3.2 Correlations for Capillary Pressure

As for the relative permeabilities, the capillary pressure curve needs to be converted to tabulated values for corresponding water saturations. There are several analytical models available in the literature, where the input parameters depend on the problem under investigation. In this work, we have chosen to use a modified version of the Skjaeveland correlation by Skjaeveland *et al.* (2000), due to its flexibility. The capillary pressure correlation is given by:

$$P_c = C_L(S_w - S_L)^{-E_L} - C_R(S_R - S_w)^{-E_R} + C_0 \qquad \text{(eq. 4.23)}$$

where C_L and C_R are capillary pressure parameters, whereas S_L and S_R are the minimum and maximum saturation parameters respectively. Furthermore, E_L is the first capillary pressure exponent, while E_R is the second capillary pressure exponent. The constant C_0 is a fitting parameter that accounts for different shapes and curvatures of the P_c-curves.

For modelling purposes, it is often convenient to convert the capillary pressure function into a dimensionless J-scaled function. J-scaling is generally used to get the same shape of the Pc-curves when the experiments have different permeability and porosity. The capillary pressure can be J-scaled according to the following equation:

$$J = \frac{1}{C_f} \cdot \frac{P_c}{\sigma} \cdot \sqrt{\frac{K}{\varphi}} \qquad \text{(eq. 4.24)}$$

where C_f is a unit conversion factor (e.g. C_f *=0.3183* for unit set: *bar, mN/m and mD).*

Chapter 5

5 Literature Experimental Data

As indicated in section 1.2, the objective of this thesis is to test if an anion exchange model can capture the behavior of the Smart water SI experiments conducted by Puntervold *et al.* (2015) represented in ***Figure 5.1***. The experimental setup is described in *section 5.1* together with core properties and dimensions. *Section 5.2* outlines the fluid properties of oil and water, in addition to the ionic composition of the FW and the different imbibing brines.

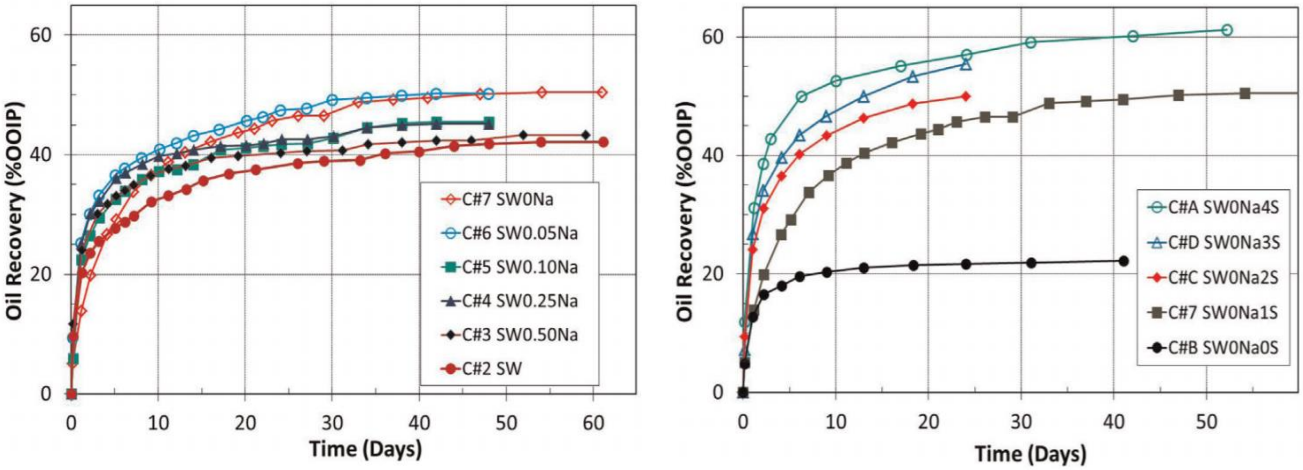

Figure 5.1 *- Oil Recovery for various Smart water SI experiments taken from Puntervold et al. (2015)*

5.1 Core Properties and Dimensions

Outcrop Stevns Klint chalk (SK) was used as the porous medium, originating from nearby Copenhagen, Denmark. The petrophysical properties and the matrix material are comparable to chalk oil reservoirs like Ekofisk and Valhall situated in the North Sea. Prior to the experiments, the cores were flushed with at least 4 pore volumes (PV) of distilled water to get rid of dissolvable salts. Then, an initial water saturation of 10% was obtained using the porous plate technique. Afterwards, the core was placed in a Hassler core holder and flooded with 2 PV of Oil A at 50 °C to establish initial oil saturation. In the end, the cores were wrapped in Teflon tape and aged at 90 °C for 3 weeks to prevent abnormal adsorption of polar components on the chalk surface (Puntervold *et al.*, 2015). The core properties are presented in ***Table 5.1***, where L is the length of the core, D the diameter of the core, V_{bulk} the bulk volume and V_{pore} the pore volume of the core respectively.

Table 5.1 *- Core Properties from Puntervold et al. (2015)*

Core	L [cm]	D [cm]	V_{bulk} [cm^3]	V_{pore} [cm^3]	φ [%]	k [mD]	S_{wi} [%]	S_{oi} [%]
SK	7.02	3.8	79.61	37.91	48	3.5	10	90

5.2 Fluid Properties

The laboratory experiments were conducted at $T = 90\ °C$ and $P = 10\ bar$ respectively. The interfacial tension (IFT) between oil and water is predicted from related fluids at comparable conditions (Fathi *et al.*, 2011a). The fluid properties of oil and water are shown in ***Table 5.2***, whereas the ionic composition of the formation water is presented in ***Table 5.3***.

Table 5.2 *- Fluid properties of oil and water from Puntervold et al. (2015)*

	μ [cP]	ρ [g/cm^3]	AN	σ [mN/m]
Oil	2.33	0.8012	0.5	13
Water	1.09	1.05	-	

Table 5.3 *- Ionic composition of the formation water from Puntervold et al. (2015)*

Ions	Concentration (mol/L)
Na^+	0.992
Ca^{2+}	0.029
Mg^{2+}	0.008
Cl^-	1.061
SO_4^{2-}	0.000
HCO_3^-	0.005
K^+	0.005

The imbibing brines used in the laboratory experiments are given in ***Table 5.4*** and ***Table 5.5*** below. ***Table 5.4*** represents the case where the imbibing brine has a varying concentration of NaCl with the definition "SWXNa". SW is an abbreviation for seawater, where "X" stands for "X" times the NaCl concentration of ordinary SW. Note that for the case "SW0Na", the NaCl concentration is not completely zero. ***Table 5.5*** describe the experiments where the brine is depleted in NaCl and spiked with 0-4 times the sulfate concentration in seawater. These experiments have the definition "SW0NaXS", where "0S" represents zero sulfate concentration, and "4S" implies four times the sulfate concentration in ordinary seawater.

Table 5.4 *– Ionic composition of imbibing brines (Puntervold et al., 2015) with varying concentration of NaCl*

Smart water used						
Ions (mol/L)	**SW**	**SW0Na**	**SW0.05Na**	**SW0.1Na**	**SW0.25Na**	**SW0.5Na**
Na^+	0.450	0.050	0.070	0.090	0.150	0.250
Ca^{2+}	0.013	0.013	0.013	0.013	0.013	0.013
Mg^{2+}	0.045	0.045	0.045	0.045	0.045	0.045
Cl^-	0.525	0.125	0.145	0.165	0.225	0.325
SO_4^{2-}	0.024	0.024	0.024	0.024	0.024	0.024
HCO_3^-	0.002	0.002	0.002	0.002	0.002	0.002
K^+	0.010	0.010	0.010	0.010	0.010	0.010

Table 5.5 *– Ionic composition of imbibing brines (Puntervold et al., 2015) depleted in NaCl and spiked with 0-4 times SO4 concentration*

Smart water used						
Ions (mol/L)	**SW**	**SW0Na0S**	**SW0Na1S**	**SW0Na2S**	**SW0Na3S**	**SW0Na4S**
Na^+	0.450	0.002	0.050	0.098	0.146	0.194
Ca^{2+}	0.013	0.013	0.013	0.013	0.013	0.013
Mg^{2+}	0.045	0.045	0.045	0.045	0.045	0.045
Cl^-	0.525	0.125	0.125	0.125	0.125	0.125
SO_4^{2-}	0.024	0.000	0.024	0.048	0.072	0.096
HCO_3^-	0.002	0.002	0.002	0.002	0.002	0.002
K^+	0.010	0.010	0.010	0.010	0.010	0.010

Chapter 6

6 Numerical Model

6.1 IORCoreSim Software (BugSim version 1.2)

IORCoreSim is used for building a 3-D model based on experimental laboratory data from Puntervold *et al.* (2015) to investigate the SI process of Smart water. The software is the second version of the *BugSim* simulator, developed at the IOR Centre of Norway (International Research Institute of Stavanger). It has the purpose of investigating oil recovery mechanisms from lab experiments and help upscale the processes to field levels. The program is extended to handle multiple components that are dissolved in the water phase, where the flow equations are solved using finite-difference discretization and a sequential solution approach for saturations and pressures. This means that the pressure field will be determined from a linear pressure equation, whilst the saturation-dependent parameters are set equal to their values at the preceding timestep. Afterwards, an additional saturation equation based on the fractional flow of water is solved, in order to update the phase velocities calculated in the first step (Lohne, 2013).

In addition, a lattice Boltzmann advection diffusion solver is used to include the geochemistry. The solver contains surface complexations, non-linear dissolution-precipitation kinetics and ion exchange, referring to the work done by Hiorth *et al.* (2012).

6.2 Numerical Setup and Simulation Input

The numerical model contains a total of 1600 grid blocks in cylindrical coordinates (20x1x80 in r, θ and z-direction respectively). Normally, the grid cells in the radial direction are divided based on the same interval, where dx is constant. This means that the first cell will have a large volume, and the volume will decrease as the number of grid cells increase. Thus, to get more representative results, it was decided to divide each grid cell based on volume instead of having a constant interval in the radial direction. This is illustrated in ***Figure 6.1***, where the first cell closest to the radial center (at r = 0 cm) is much wider than the last cell (at r ~ 1.9 cm), corresponding to equal cell volume.

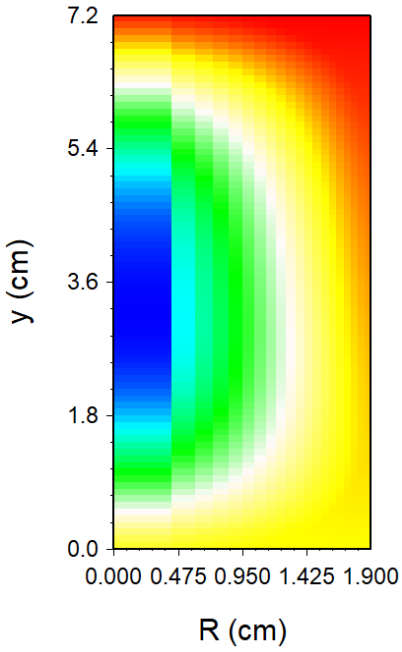

Figure 6.1 *- Visualization of grid cells in radial direction*

The main input parameters necessary to run the simulator are as follows:

- Core properties and dimensions (porosity, permeability, diameter, length)
- Fluid properties (density, viscosity, oil/water interfacial tension)
- Imbibing brines (ionic compositions)
- Saturation functions (relative permeability, capillary pressure)

6.3 Saturation functions

The model implemented in IORCoreSim aims to capture the wettability alteration from a system with initial wetting towards a more water-wet system. Thus, two saturation functions are required that explains these two scenarios.

6.3.1 Relative Permeability curves

The relative permeability curves for water and oil are developed using modified Corey correlations corresponding to *eq. 4.21* and *eq. 4.22* respectively. Since there is not enough information to independently determine the functions for both the initial system and a more water-wet system, it was decided to keep the curves constant and vary Pc instead. Corey exponents used to establish the curves are shown in ***Table 6.1***, while the relative permeability curves are presented in ***Figure 6.2***.

Table 6.1 *- Corey exponents used to develop relative permeability curves*

k_{rw}*	k_{ro}*	n_w	n_o	S_{wi}	S_{or}
0.57	1.00	4.70	2.20	0.073	0.13

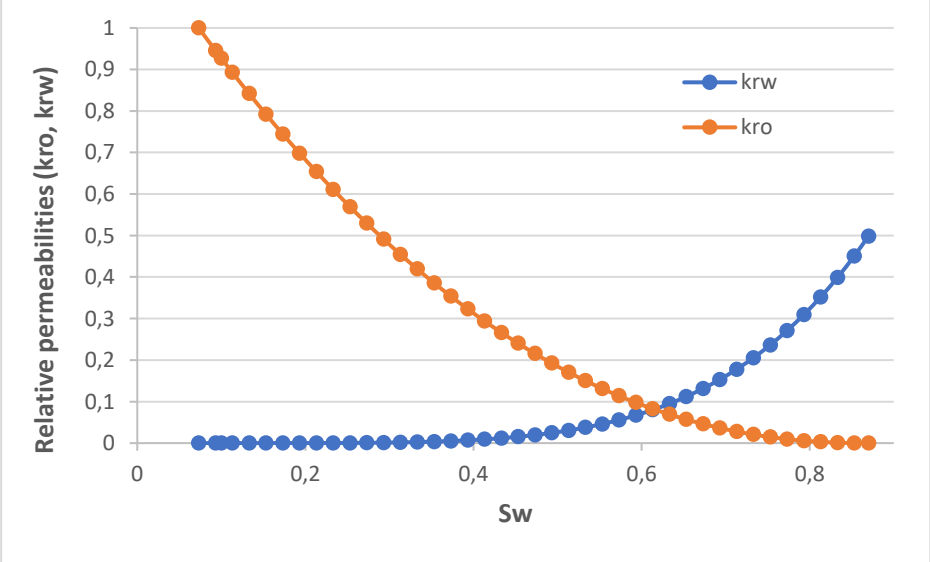

Figure 6.2 *- Relative permeability curves for oil and water*

6.3.2 Capillary Pressure curves

The capillary pressure curves are based on the experiments executed by Webb *et al.* (2005). The study was performed on a core at reservoir conditions analogous to the North Sea Valhall field. Capillary pressure tests were utilized during two imbibition tests, one with formation water (SFW) and the other with sea water (SSW) as the displacing fluid. For simulation purposes, it is convenient to express the capillary pressure curves as an analytical function. The capillary pressure curve obtained by flooding a core with Valhall formation brine (SFW) is J-scaled according to *eq. 4.24*. The result, J-experimental, is shown in ***Figure 6.3*** together with the correlated J-function used to match the experimental. The correlated J-function is calculated using modified Skjaeveland's correlations corresponding to *eq. 4.23*.

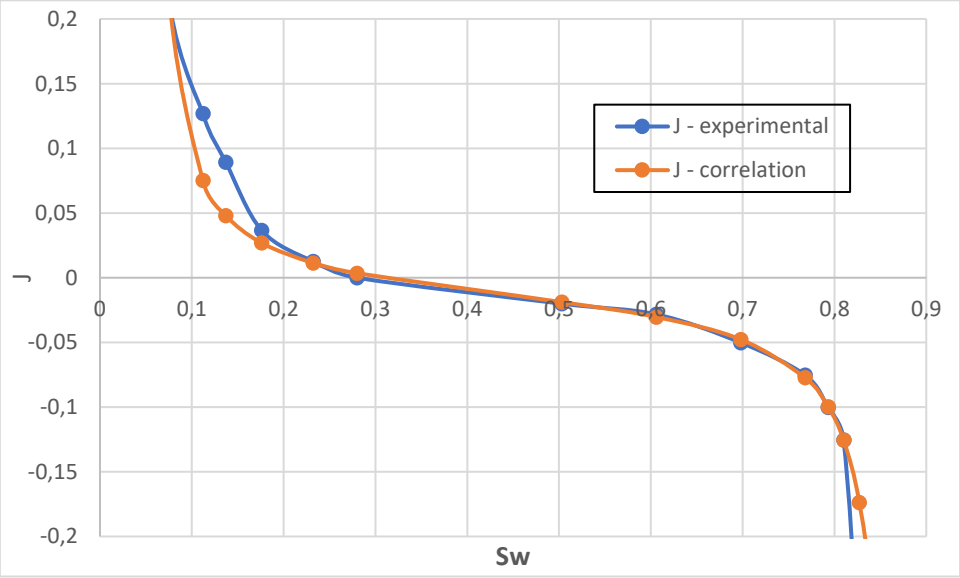

Figure 6.3 *- J-scaled capillary pressure curves for experimental formation water (J-experimental) and calculated formation water (J-correlation)*

Since SO_4^{2-} is assumed to be the wettability alternating agent, an imbibing brine without sulfate will represent the initial wetting of the core. Seeing that the formation water in the experiments carried out by Webb *et al.* (2005) contained zero SO_4^{2-} concentration, it is possible to compare the corresponding capillary pressure curve with the case "SW0Na0S" from Puntervold *et al.* (2015). It was decided to tune the "J-correlation" capillary pressure curve and lower the

curvature to obtain a slower imbibition rate of the formation brine. The tuned capillary pressure curve "J1", which will be used in the "SW0Na0S" simulation, is shown in ***Figure 6.4***.

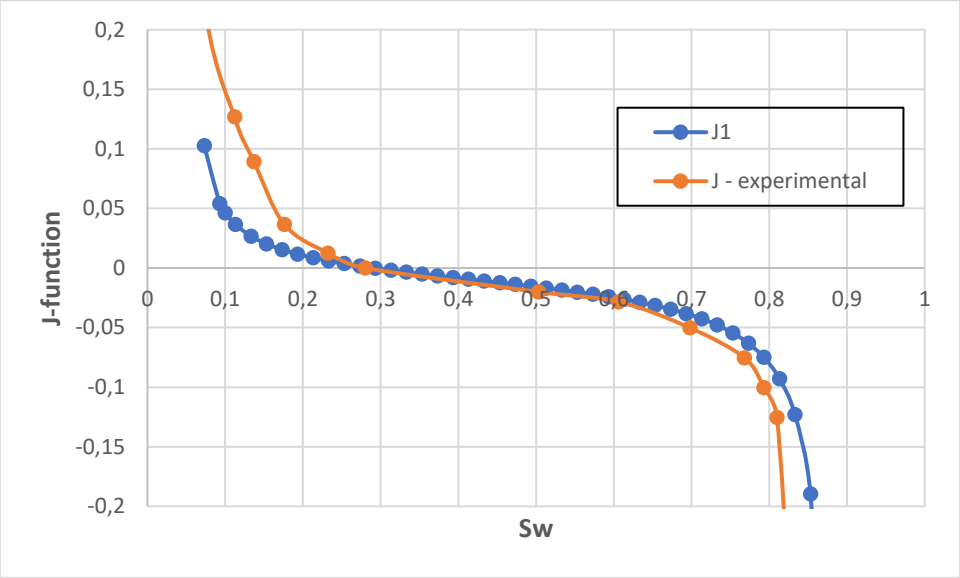

Figure 6.4 *- J-scaled capillary pressure curves for experimental formation water (J-experimental) and tuned calculated formation water (J1)*

Given that the model requires two saturation tables to capture a wettability alteration, another capillary pressure curve needs to be defined. In a more water-wet system, Pc will reach zero at a higher S_w compared to a less water-wet system. Since there is not enough information to determine this function, it was decided to raise the capillary pressure curve in ***Figure 6.4*** by approximately 50 mBar, while keeping the curvature constant. This resulted in the second capillary pressure curve referred to as "J2", which will be used as an estimate of representing a more water-wet system. ***Figure 6.5*** illustrates the capillary pressure curves that will be used in the model, namely "J1" for the initial wetting system and "J2" for a more water-wet system respectively. ***Figure 6.6*** illustrates the same capillary pressure curves, but in the unit mBar instead of J-function. Modified Skjaeveland's correlations used to establish the curves are shown in ***Table 6.2***.

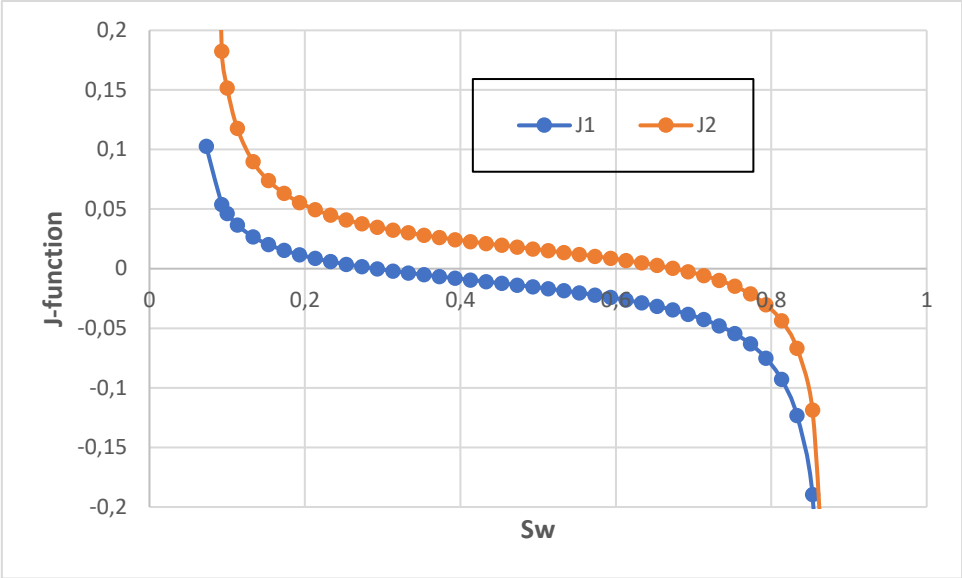

Figure 6.5 *- Calculated J-function for a less-water wet state (J1) and a more water-wet state (J2)*

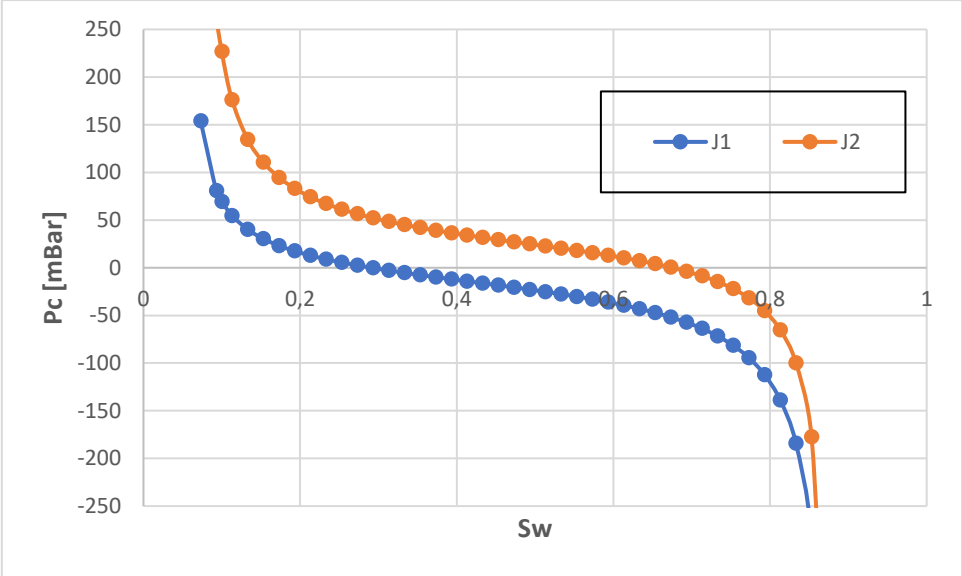

Figure 6.6 *- Calculated Pc-curves for a less-water wet state (J1) and a more water-wet state (J2)*

***Table 6.2** - Modified Skjaeveland's correlations used to compute the Pc-curves*

	C_L	C_R	C_0	E_L	E_R	S_L	S_R
J1	0.014	0.013	-0.0102	0.51	0.75	0.06	0.88
J2	0.013	0.008	0.01	0.70	0.080	0.07	0.88

6.4 Imbibition velocity of imbibing brines

One of the main challenges in matching the experimental oil recoveries from Puntervold *et al.* (2015) is to get a correct imbibition velocity of the imbibing brines. As is evident in ***Figure 5.1***, the brine without chemistry "SW0Na0S" seems to have a lower SI rate compared to the cases where a WA agent is present in the brine. Thus, the model need to be modified to capture the correct imbibition velocity of the imbibing brines when sulfate is present.

It is believed that the imbibition rate depends on the capillary pressure of the system and the relative permeabilities of oil and water. Thus, one option is to change the Pc-curve in the same way as for the initial case "SW0Na0S". However, making an artificial flat Pc-curve is very difficult since the model interpolates between "J1" and "J2" when the imbibing brine contains sulfate. Another option is to reduce the relative permeabilities of oil and water. The contribution of water and oil is investigated by plotting the distribution of P_w and P_o at early time as illustrated in ***Figure 6.7*** and ***Figure 6.8***.

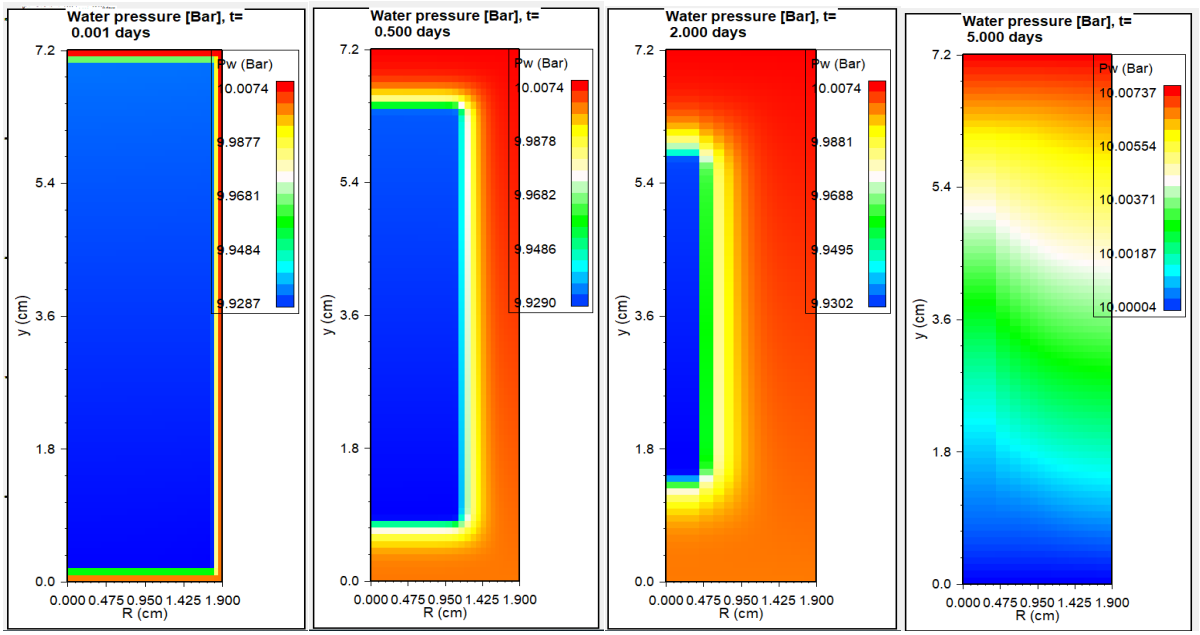

Figure 6.7 *- Illustration of P_w [bar] distribution in the core at t=0.001 days, t=0.5 days, t=2 days and t=5 days respectively*

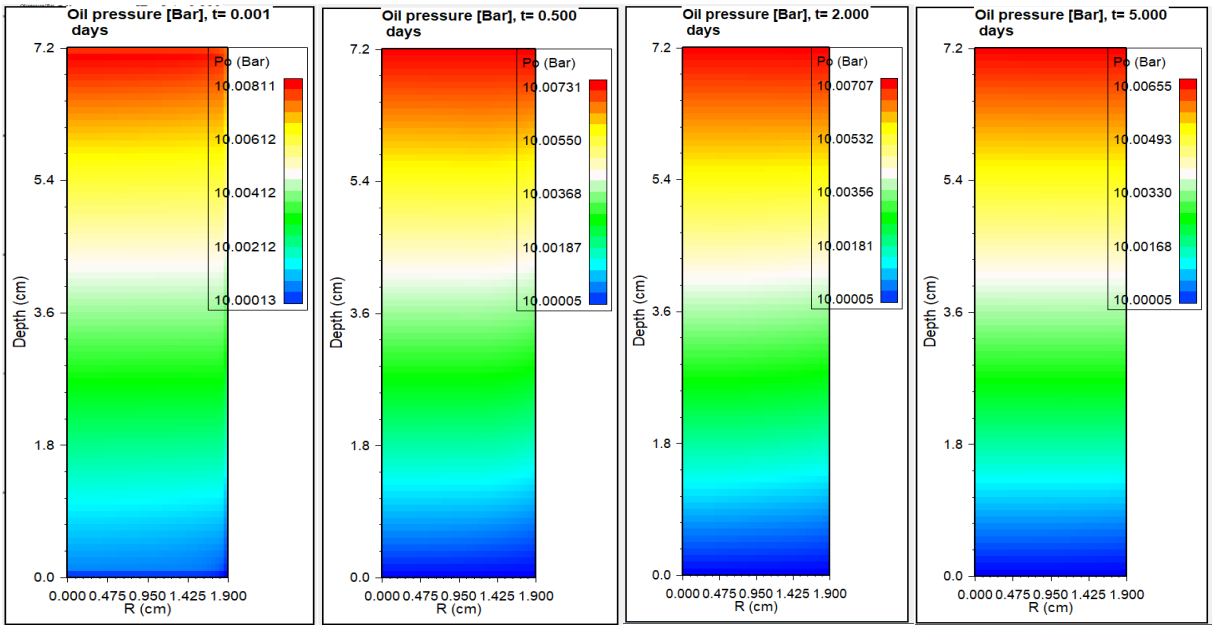

Figure 6.8 *- Illustration of P_o [bar] distribution in the core at t=0.001 days, t=0.5 days, t=2 days and t=5 days respectively*

As is apparent from ***Figure 6.7*** and ***Figure 6.8***, there is a high gradient in the water pressure when the imbibition starts. Contrary, the oil pressure has almost a zero gradient, which means that it is the λ_w and P_c (S_{wi}) that controls the production rate. Thus, it would be natural to reduce the relative permeability curve of water to obtain a slower imbibition velocity of the brines. However, reducing k_{rw} with a factor ten would give unrealistic results. Therefore, a reasonable choice is to assume that the oil recovery rate is restricted by the diffusion velocity of sulfate into the core. The diffusion model implemented in IORCoreSim follow the subsequent relation:

$$J_i = \nabla C_{w,i} D_{w,i} \varphi^m S_w^{n_w} \qquad \text{(eq. 6.1)}$$

where J_i is the diffusive flux of a diffusing component *i* travelling with the water phase *w*, *D* the bulk diffusion coefficient, *m* the cementation exponent (between 2.0 – 2.6 for carbonates) and *n* the saturation index for water (between 2.0 – 3.0 for mixed-wet systems).

It is useful to first estimate the diffusion coefficient in the systems without chemistry and further lower this value to capture the imbibition velocity of the brines containing sulfate. When no chemistry is added to the model, the process is capillary driven, and diffusion follow the last term of *eq. 4.11* corresponding to:

$$D_c(S_w) = -K\lambda_o f_w \nabla P_c \qquad \text{(eq. 6.2)}$$

where D_c is the capillary diffusion coefficient at various water saturations. The gradient in capillary pressure can be determined for both the first and the second saturation function based on the numerical derivative of P_c:

$$\frac{\partial P_c}{\partial S_w} = \frac{P_c(S_{w1}) - P_c(S_{w2})}{S_{w1} - S_{w2}} \qquad \text{(eq. 6.3)}$$

Figure 6.9 depicts the calculated diffusion coefficients for the systems without chemistry, where *Dc1* is calculated by using "J1" and *Dc2* is calculated by using "J2" with corresponding relative permeability values.

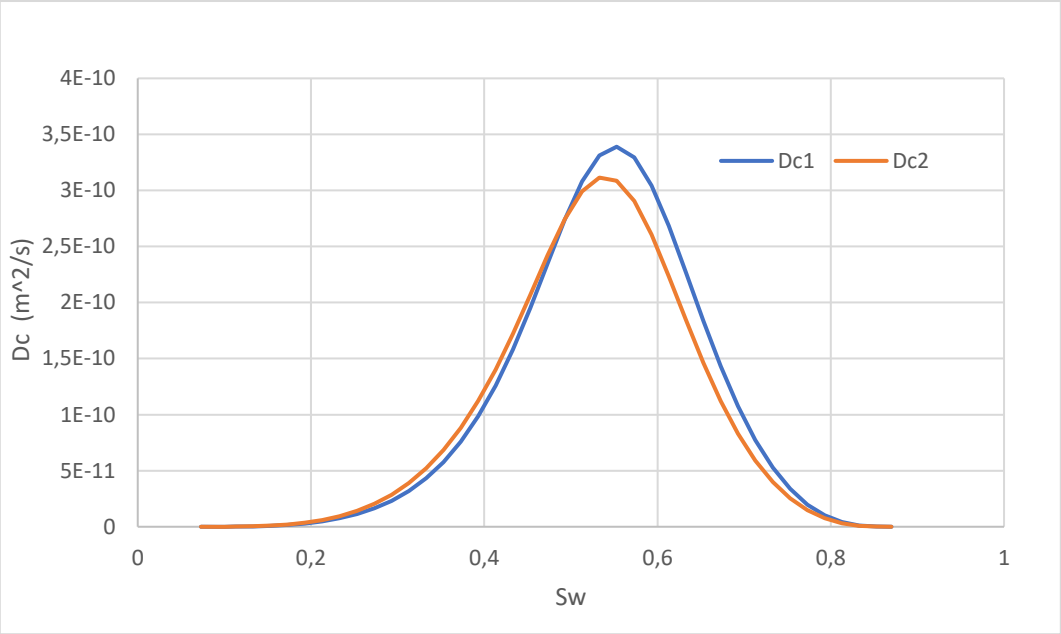

Figure 6.9 *- Diffusion coefficients for systems without chemistry: Dc1 (corresponding to saturation table one) and Dc2 (corresponding to saturation table two) respectively*

If we assume that $D_c = 2.5 \cdot 10^{-10} \frac{m^2}{s}$ referring to ***Figure 6.9***, the time it takes to reach recovery can be calculated based on a simplified version of the analytical solution to the well-known Fick's 2nd law, where *L* is the distance to the center of the core:

$$t = \frac{L^2}{4 \cdot D} \qquad \text{(eq. 6.4)}$$

$$t = \frac{(0.019m)^2}{4 \cdot 2.5 \cdot 10^{-10} \frac{m^2}{s}} \cdot \frac{1.16 \cdot 10^{-5}\ days}{s} = 4.2\ days \qquad \text{(eq. 6.5)}$$

According to the experimental data under investigation (Puntervold *et al.*, 2015), it takes tens of days or even months to reach the recovery when the imbibing brine contains sulfate. Thus, it was decided to assume that the diffusion coefficient should be reduced with a factor 10-100, corresponding to $D = (10^{-11} - 10^{-12}) \frac{m^2}{s}$.

6.5 Adsorption Isotherm

The ion exchange capacities for positive and negative surface sites are presented in ***Table 6.3***. X^- is just a selected value, whereas Z^+ was chosen high enough to reduce the diffusion velocity of sulfate into the core.

Table 6.3 *- Ion exchange capacity for Z^+ and X^-*

Surface site	Ion exchange capacity (mol/L PV)
Z^+	0.2
X^-	0.15

To determine the adsorbed amount of sulfate ions in the different cases, each of the experiments in ***Figure 5.1*** are simulated and run for one timestep. IORCoreSim will then create a datafile that gives information about the initial solution of the system, and particularly the fraction of sulfate that occupies the available positive surface sites. Based on the equivalent fraction of SO_4^{2-} and the anion exchange capacity (Z^+), the adsorbed amount of sulfate is determined based on *eq. 6.6*. This is done for all the experiments, and the results are shown in ***Table 6.4***.

$$\rho_{SO4}^{s} = \frac{Z^{+} * equivalent\ fraction\ of\ SO_4^{2-}}{\text{valence number of } SO_4^{2-}} \qquad \text{(eq. 6.6)}$$

Table 6.4 *- Adsorbed amount of SO4 (mol/L) for the different Smart Water SI experiments*

Case	ρ_{SO4}^{s} (mol/L PV)
SW	0.019
SW0.5Na	0.033
SW0.25Na	0.045
SW0.1Na	0.054
SW0.05Na	0.058
SW0Na	0.062
SW0Na0S	0.000
SW0Na1S	0.062
SW0Na2S	0.073
SW0Na3S	0.078
SW0Na4S	0.081

By using the keyword *"ncmisc"* in the model, the interpolation parameter *"Fm"* is triggered, which is used to interpolate between two sets of saturation functions according to *eq. 4.20*. "*Fm"* needs to be entered as a table together with adsorbed amount of sulfate (ρ^s_{SO4}), where the interpolation parameter is the weighing of saturation table number two. As the concentration of adsorbed sulfate increases, the system moves towards a more water-wet wetting state, and more oil can be retrieved from the core. The interpolation parameter is defined for all the cases based on *eq. 6.7* and *eq. 6.8* below.

$$Fm = \frac{0 - P_{c1}\,(Sw_{end})}{P_{c2}(Sw_{end}) - P_{c1}(Sw_{end})} \qquad \text{(eq. 6.7)}$$

$$Fm = \frac{a}{a+b} \qquad \text{(eq. 6.8)}$$

where the constants *a* and *b* are visualized in ***Figure 6.10***, $P_{c1}\ (Sw_{end})$ and $P_{c2}\ (Sw_{end})$ are the capillary pressure at the water saturation endpoint. Sw_{end} is found by estimating the recovery of the experiments from ***Figure 5.1*** and then use the value in the equation below.

$$Sw_{end} = Recovery\ x\ (1 - S_{wi}) + S_{wi} \qquad \text{(eq. 6.9)}$$

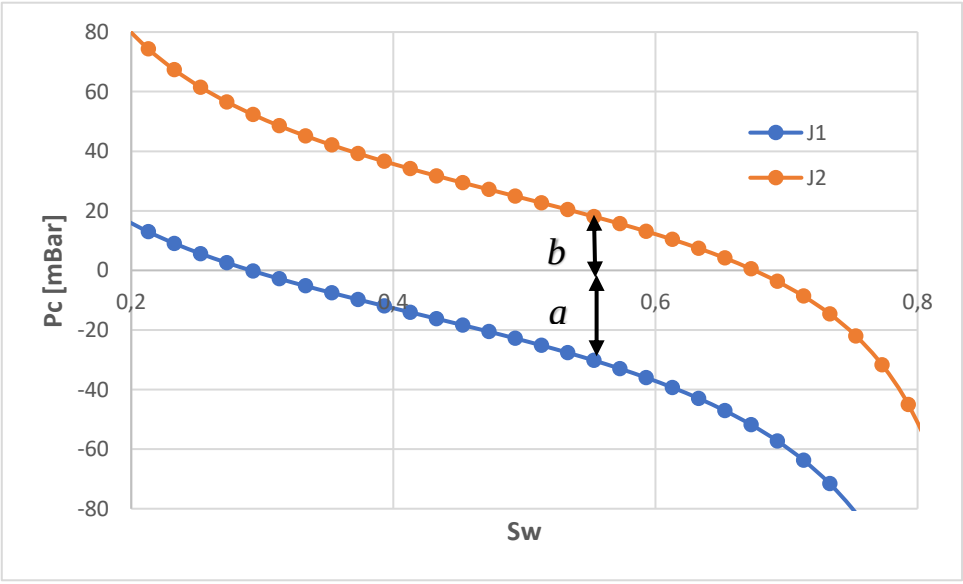

Figure 6.10 *- Visualization of how to define the interpolation parameter from the Pc-curves*

The final adsorption isotherm applied in the model is described in ***Table 6.5***. Note that even though the anion exchange capacity was set equal to 0.2 mol/L, the table extends from 0 – 0.1 mol/L. This is because adsorption of 1 SO_4 will occupy 2 surface sites, referring to *eq. 3.11.*

Table 6.5 *- Adsorbed amount of SO_4^{2-} versus miscibility parameter Fm*

ρ^s_{SO4} *(mol/L)*	***Fm***
0.000	0.017
0.019	0.443
0.033	0.474
0.045	0.507
0.054	0.528
0.058	0.618
0.062	0.641
0.062	0.641
0.073	0.618
0.078	0.739
0.081	0.936
0.100	1.000

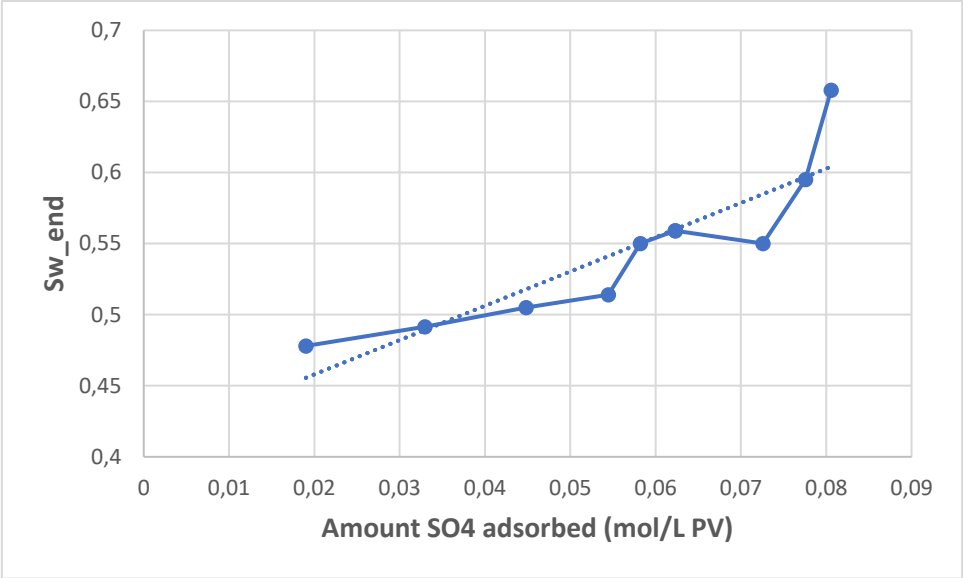

Figure 6.11 *– Amount of SO_4^{2-} adsorbed vs. endpoint water saturation used to develop Fm table in the model*

Figure 6.11 illustrates the adsorbed amount of sulfate vs. endpoint water saturation that was used to develop the interpolation table in the model. The y-axis is independent of the model since it only describes the endpoint saturation retrieved from the experimental data. However, the x-axis will depend on the model for adsorption, and another model will most likely give different results. Nevertheless, there is a relative monotony relation between $S_{w,end}$ and the amount of sulfate adsorbed on the chalk surface. The stippled line illustrates an estimated regression line, but the data points were used as input values in the model.

Chapter 7

7 Results and Discussion

7.1 SI in a system with fixed wettability

As wettability alteration is assumed to be one of the main mechanisms in a SI Smart water process, it is useful to first interpret the case corresponding to a system with fixed wettability. As was outlined in the introduction of this thesis, an oil-wet rock will hold more strongly onto the oil compared to a water-wet rock. If the imbibing brine can alter the wettability, the recovery profile should be comparable to that of a more water-wet system. ***Figure 7.1*** depicts the estimated recovery of a chalk core with fixed wettability corresponding to a more water-wet state. The simulation is run without chemistry where only the second saturation function is used, namely "J2". The predicted SI was initiated almost immediately, and a recovery of 65 % after ~ 0.3 days is expected.

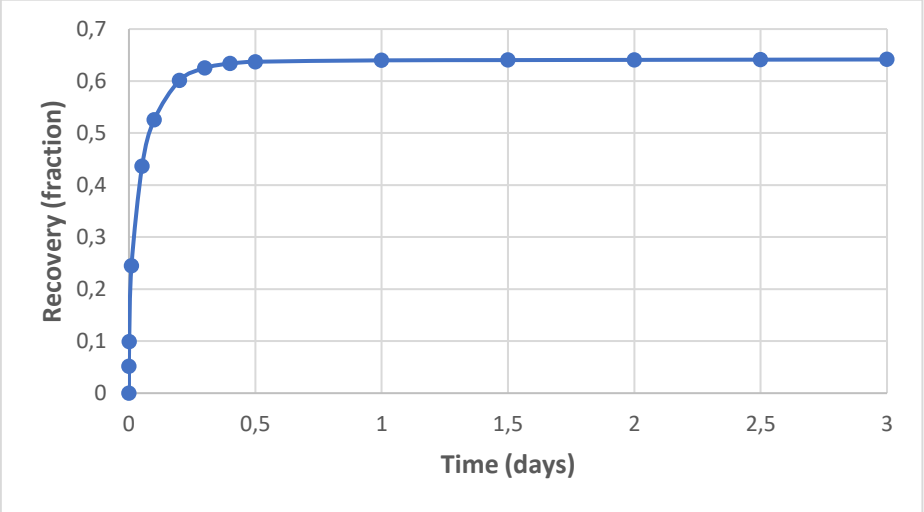

Figure 7.1 *- Expected recovery for a system with fixed wettability*

7.2 History matching experimental data

The following section provides the history matching between simulated and experimental oil recoveries. The results are presented and discussed in terms of the proposed Smart water mechanisms in carbonate reservoirs.

7.2.1 Matching SWXNa – experiments

Figure 7.2 illustrates the matching of simulated and experimental oil recoveries during spontaneous imbibition of "SWXNa" brines. As is apparent from the figure, there is a small deviation in the time it takes to reach plateau. This is particularly the case for SI of ordinary SW, where experimental data gives an oil recovery plateau after 45 days in contrast to a simulated plateau after 30 days. Even though the imbibition velocity of the brines was reduced by lowering the diffusion coefficient of ions, the effect of too high imbibition velocity may still be a limitation of the anion exchange model. This will be discussed further in *section 7.5.1*.

Even though there is a slight difference in the imbibition rates, the simulated curves capture the most important recovery trends of the experimental data. As is evident in ***Figure 7.2***, oil recovery of 42 % is achieved in both cases during SI of ordinary SW into the chalk core. When the NaCl concentration of the imbibing brine is reduced, the oil recovery gradually increases. The plateau recovery for the brine depleted in NaCl (SW0Na) is 50 %, which is an 8 % increase compared to ordinary SW.

The anion exchange model couple wettability alteration to the adsorbed amount of sulfate at the chalk surface. Consequently, the system will move towards a more water-wet state as the sulfate adsorption increases. However, the experimental data in ***Figure 7.2*** show that the concentration of sulfate is unchanged, but the recovery increases through the experiments. Accordingly, there must be another mechanism that can explain the extra oil retrieved from the core in an anion exchange process. The formation water and the imbibing brines consist of three anions, namely Cl^-, HCO_3^- and SO_4^2. As the Cl^- concentration decreases through the experiments, there is less competition between the anions in the system. Correspondingly, it will be easier for SO_4^{2-} to adsorb onto the chalk surface when the concentration of chloride is reduced, referring to ***Figure 7.3.*** Thus, the anion exchange model can predict the experimental recoveries, even though the sulfate concentration is kept unchanged.

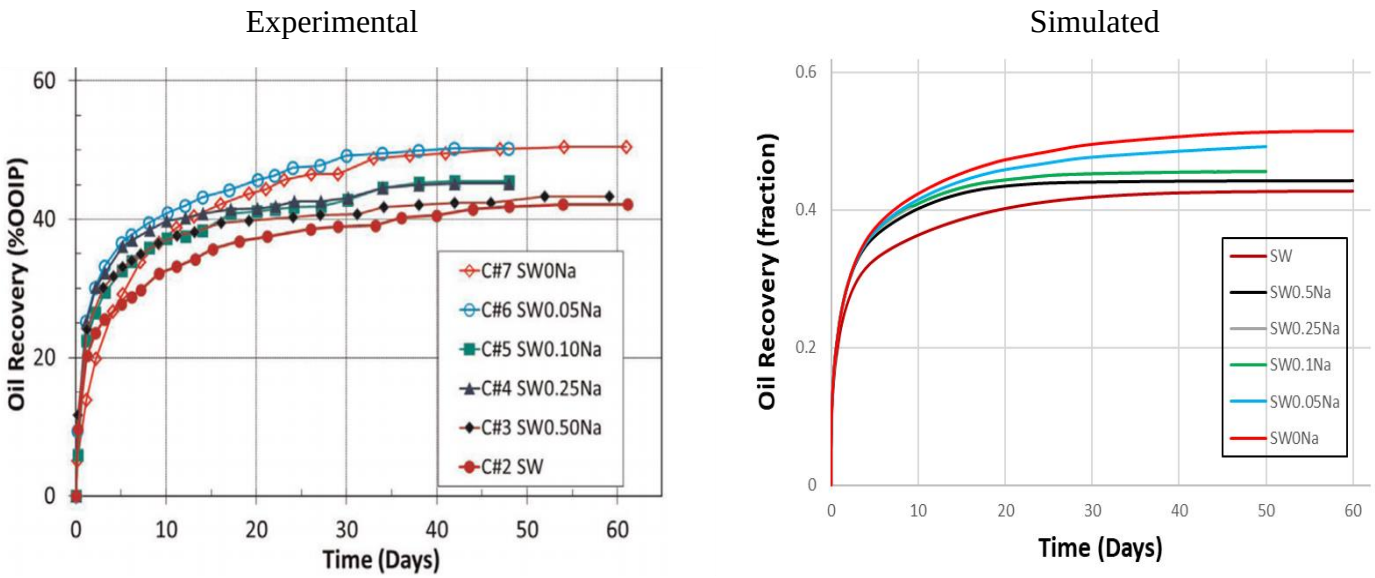

Figure 7.2 *– SI of Smart water brines with varying concentration of NaCl.*
Left: experimental recoveries (Puntervold et al., 2015) and Right: simulated recoveries

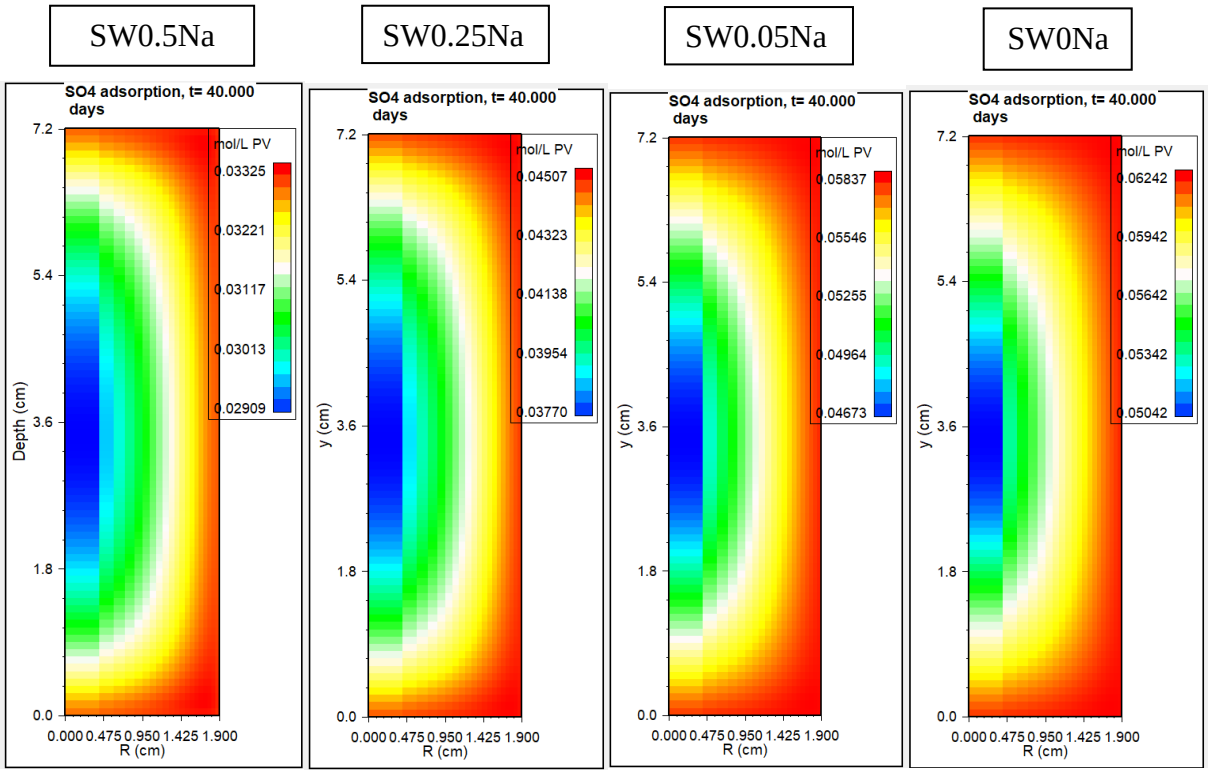

Figure 7.3 *- Visualization of ρ^{s}_{SO4} at t=40 days for the imbibing brines SW0.5Na, SW0.25Na, SW0.05Na and SW0Na respectively*

According to Qiao *et al.* (2016), a high concentration of NaCl in the imbibing brine may reduce the Smart water effect in two ways. Firstly, all charged surfaces in acquaintance with a brine will have an excess of ions near the surface, which was outlined in *section 3.3* and is known as the electrical double layer. Since Na^+ and Cl^- does not contribute active in the wettability alteration process, access of the potential determining ions SO_4^{2-}, Ca^{2+} and Mg^{2+} to the chalk surface will be slightly obviated. This results in less attraction between the chalk surface and the potential determining ions, corresponding to a reduction in surface adsorption and a decline in the amount of carboxylic material released. ***Table 7.1*** signifies that the concentration of NaCl is much higher in seawater compared to SO_4^2, Ca^{2+} and Mg^{2+}. Correspondingly, SW depleted in NaCl should act as a smarter water compared to ordinary SW. This observation is well recognizable in ***Figure 7.2***, where SW0Na gives an 8 % higher oil recovery compared to ordinary SW.

Secondly, Na^+ and Cl^- can form aqueous complexes with SO_4^{2-}, Ca^{2+} and Mg^{2+}, referring to *eq. 3.4 – 3.6.* When aqueous complexes form, the free-ion concentration feasible to adsorb on the surface is lowered. Accordingly, reducing the concentration of NaCl can benefit the adsorption of potential determining ions and correspondingly give an increase in oil recovery.

7.2.2 Matching SW0NaXS – experiments

Figure 7.4 illustrates the history matching of oil recoveries during spontaneous imbibition of "SW0NaXS" brines, where the concentration of sulfate is changed through the experiments. As is apparent from the figure, a relatively good match is obtained for the case "SW0Na0S" with a recovery of 22 %. The system is representative of the initial wetting of the core, as it does not contain any wettability alternating properties. When sulfate is added to the imbibing water, corresponding to "SW0Na1S", the oil recovery instantly increases from 22 % to 50 % of the OOIP. However, the spontaneous imbibition is slightly too fast, which again may be one of the limitations of the model.

A deviation between simulated and experimental "SW0Na3S" is also apparent from the figure. It appears that the experimental curve would have reached a recovery comparable to "SW0Na4S" if the experiments were carried out for a longer period. In comparison, there is a 7 % difference in oil recovery between the simulated "SW0Na3S" and "SW0Na4S". The difference between experimental and simulated results may be caused by an experimental uncertainty, but since the experimental data ends after 25 days, it is difficult to give a precise prediction of the behavior of the curve. Nevertheless, the overall match between the simulated and the experimental data is satisfactory and captures the main trends of the recovery profiles.

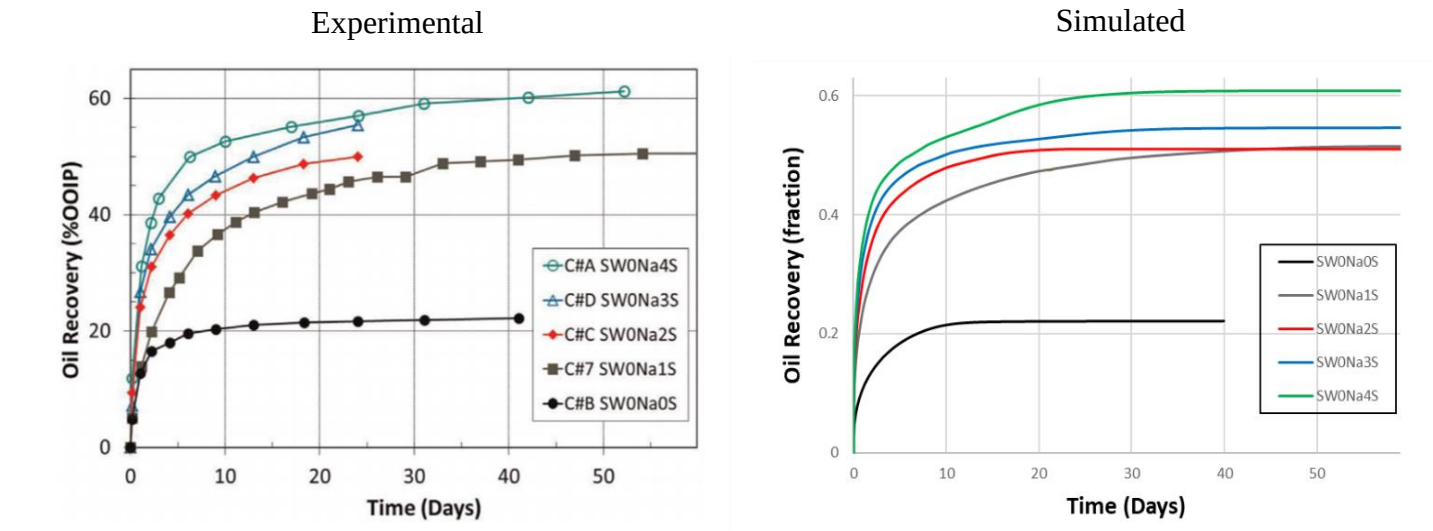

Figure 7.4 *- SI of Smart water brines depleted in NaCl and spiked with 0-4 times SO4 concentration of SW. Left: experimental recoveries (Puntervold et al., 2015) and right: simulated recoveries*

As was outlined in *section 3.2*, sulfate acts as a catalyst for the wettability alteration process towards a more water-wet system. Therefore, the effectiveness of the process is highly determined by the access of SO_4^{2-} ions towards the chalk surface. When the imbibing brine is depleted in NaCl, the ionic double layer is primarily expressed by potential determining ions. Thus, the access of sulfate to the calcite surface is enhanced. As the concentration of SO_4^{2-} in the imbibing brine increases, more sulfate is exchanged against other anions detached to the surface in an anion exchange process. Accordingly, as the amount of ρ_{SO4}^{S} increases, the system moves towards a more water-wet state and a greater amount of oil is expelled from the chalk core. According to Fathi *et al.* (2011b), the optimal sulfate concentration corresponding to the highest possible oil recovery, is dependent on the initial Ca^{2+} concentration in addition to temperature. These effects will be discussed more thoroughly in *section 7.5*, where possible limitations of the model are examined.

7.3 Other possible Smart water mechanisms

It should be emphasized that the anion exchange model does not account for other Smart water mechanisms such as precipitation and dissolution of minerals. However, these reactions may have an important role in the SI process and will be outlined in more detail below.

Precipitation and Dissolution reactions

Hiorth *et al.* (2010) investigated how pore water chemistry can impact carbonate rocks and change the wettability of the system. They implemented a chemical model that couples surface and aqueous chemistry with dissolution and precipitation reactions in carbonates. In the temperature range investigated (70 – 130 ℃), they found that dissolution of calcite and precipitation of anhydrite may occur in SK chalk cores. In the lower temperature range, the imbibing brine is in equilibrium with the chalk surface. However, when the temperature is increased, Ca^{2+} will react with SO_4^{2-}, which causes $CaSO_4$ (s) to precipitate. As the system wants to remain in equilibrium with $CaCO_3$ (s), calcium needs to be supplied to the system and dissolution may take place referring to *eq. 3.2*. Their findings are presented below in ***Figure 7.5***.

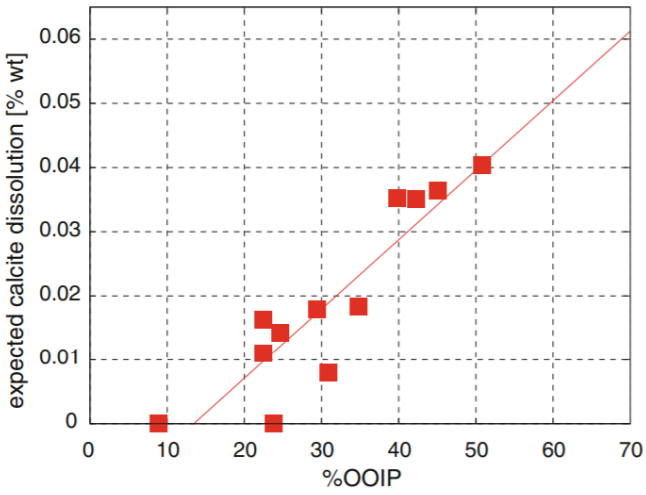

Figure 7.5 *- Expected calcite dissolution vs. %OOIP taken from Hiorth et al. (2010)*

As is apparent from ***Figure 7.5***, the expected calcite dissolution correlates linearly with oil recovery experiments executed by Zhang and Austad (2006). The cores were initially saturated with Ekofisk brine, whereas seawater at temperatures between 70 – 130 ℃ spontaneously imbibed and expelled oil from the core. Their findings indicate that dissolution of calcite could be linked to a higher oil recovery, if the process takes place where the organic matter is adsorbed.

Puntervold *et al.* (2015) claims that it is not feasible to spike the imbibing water with SO_4^{2-} at temperatures above 100 °C due to possible precipitation of anhydrite referring to *eq. 3.3.* Precipitation of anhydrite is unwanted due to the reduction in permeability of the chalk and blocking of pores. It is commonly known (Austad, 2013) that the solubility of $CaSO_4$ (s) decreases as the temperature increases. However, the experiments investigated in this thesis are executed under a relatively low temperature compared to other carbonate fields in the North Sea. Thus, at a reservoir temperature of 90 °C, precipitation of anhydrite should not affect the final oil recoveries.

7.4 Scaling

According to Stoll *et al.* (2008), imbibition of water after a wettability alteration process will be limited to the diffusion of ions. The paper claims that spontaneous imbibition after a WA process will take ~1000 times longer compared to SI of water into a more water-wet medium. The reason is that the wettability alternating water must diffuse into the rock and make it more water-wet before a SI process takes place. Stoll *et al.* (2008) claims that it could take up to 200 years before the same recoveries are achieved from a $1m^3$ matrix cube, compared to a centimeter-scale core plug in a 100 days period at the laboratory.

Possible scaling problems can be investigated by looking at the link between diffusion and time, given by the simplified version of the analytical solution to Fick's 2nd law, which was outlined in *section 6.4.* It was assumed that $D = 2.5 \cdot 10^{-10}\ m^2/s$ in a system without chemistry, but since it seems that sulfate limits how fast the SI process goes, it was decided to lower the diffusion by a factor 10-100 by introducing Archie exponents *m* and *n*.

If we assume that $D = 10^{-11}\ m^2/s$ and the matrix block is $1\ m^3$ *(center of block is L = 0.5 m.),* we can estimate the time it takes for the brines to diffuse into the rock:

$$t = \frac{(0.5m)^2}{4 \cdot 10^{-11} \frac{m^2}{s}} \cdot \frac{3.17 \cdot 10^{-8}\ years}{s} = 198\ years \qquad \text{(eq. 7.1)}$$

In comparison, for a core with $r = 0.019\ m$ and $D = 10^{-11}\ m^2/s$, the estimated diffusion time is:

$$t = \frac{(0.019\ m)^2}{4 \cdot 10^{-11} \frac{m^2}{s}} \cdot \frac{3.8 \cdot 10^{-7}\ months}{s} = 3.4\ months \qquad \text{(eq. 7.2)}$$

Since the time of diffusion increases with the square root of distance, diffusion in a larger matrix block can take hundreds of years compared to diffusion in cores at the laboratory. For upscaling purposes, this implies that the imbibing Smart water need to have an effective transport mechanism to be economically feasible as an EOR method.

7.5 Limitations of the model

In the following section, possible limitations of the anion exchange model will be discussed. Special focus will be on diffusion velocity of ions, anion exchange capacity, changes in temperature, oil chemistry and the impact of modifying the Ca^{2+} concentration.

7.5.1 Diffusion velocity

The current diffusion model implemented in IORCoreSim is represented by *eq. 6.1*. The equation includes diffusion of a component dissolved in the water phase and is restricted to represent only non-polar species. However, according to the study done by Samson *et al.* (2003), the diffusion of ions also depend on the gradient of electrical potential and the activities of the ions. The relation is presented in *eq. 7.3* below.

$$J_i = -\theta D_i \frac{\partial C_i}{\partial x} - \theta \frac{D_i z_i F}{RT} C_i \frac{\partial \psi_i}{\partial x} - \theta D_i C_i \frac{\partial ln\gamma_i}{\partial x} + C_i V_x \qquad \text{(eq. 7.3)}$$

where

J_i = bulk ionic flux

C_i = concentration of species *i*

θ = volumetric water content in the pores

ψ = electrical potential

z_i = valence number of species *i*

F = Faraday constant

R = ideal gas constant

γ_i = activity coefficient of species *i*

V_x = bulk velocity of fluid

According to *eq. 7.3*, the gradient in electrical potential and the activity of SO_4^{2-} may also contribute to the effective diffusion of sulfate. This means that the current diffusion model in IORCoreSim (*eq. 6.1)* may be insufficient as it gives a too high diffusion rate of ions, corresponding to a deviation in the time it takes to reach plateau in simulated oil recoveries.

7.5.2 Anion exchange capacity

The anion exchange capacity (Z^+) used in the model is equal to 0.2 mol/L PV. The following section will address whether this is a realistic value or not.

An upper limit for the number of free sites on the surface (CEC) can be defined by estimating the amount of $CaCO_3$ ions at the surface. First, the shape of $CaCO_3$ ions is assumed to be cubic so that their sides (ds) can be computed by *eq. 7.4*. Then the number of ions/m^2 is calculated based on *eq. 7.5*, followed by a conversion to the number of ions/L PV corresponding to *eq. 7.6*. It is assumed that the specific surface area (S_0) of SK chalk is ~ 2 m^2/g, and that the molecular weight (M_w) is 100 g/mole. Avogadro's constant (N_A) is the number of molecules in one mole and has the value $6.022 \cdot 10^{23}$.

$$ds = \left(\frac{M_{w,CaCO_3} \cdot \frac{1}{N_A}}{\rho_{CaCO_3}} \right)^{\frac{1}{3}} \quad \text{(eq. 7.4)}$$

$$\frac{ions}{m^2} = \frac{\frac{1}{N_A}}{ds^2 \cdot 10^{-4}} \quad \text{(eq. 7.5)}$$

$$CEC = S_0 \cdot \rho \cdot \left(\frac{1-\varphi}{\varphi} \right) \cdot 10^3 \cdot \frac{ions}{m^2} \quad \text{(eq. 7.6)}$$

The estimated maximum CEC based on *eq. 7.6* has a value of 0.07 mole/L PV. This should correspond to the sum of both Z^+ and X, representing both positive and negative free surface sites. Thus, the calculations indicate that the value used in the model is unrealistically high.

The validity of the anion exchange capacity can also be discussed based on other experimental data. Strand *et al.* (2006a) investigated how sulfate adsorbs onto the chalk surface by looking at effluent profiles from chromatographic tests. In their studies, they considered SK cores that were initially 100 % saturated with brine without sulfate. The initial brine was displaced by seawater containing both tracer (SCN^-) and SO_4^{2-} at a concentration of 0.024 mol/L. The test was performed at 100 ℃ and the result is shown in ***Figure 7.6*** below.

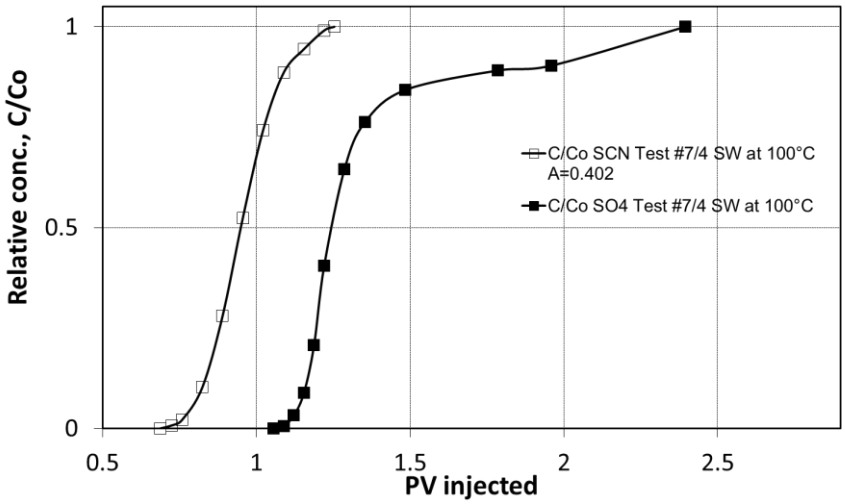

Figure 7.6 *- Chromatographic test of sulfate adsorption in SK chalk at 100C retrieved from Strand et al. (2006a)*

By measuring the offset in the effluent profiles between SCN^- and SO_4^{2-} from ***Figure 7.6***, it is possible to estimate the amount of sulfate adsorption on the chalk surface. SO_4^{2-} appear ~ 0.3 PV later than SCN^-, which means that ρ_{SO4}^s is equal to:

$$\rho_{SO4}^s = 0.3 \text{ PV} \cdot 0.024 \frac{\text{mol}}{\text{L}} = 0.0072 \frac{mol}{L} \qquad \text{(eq. 7.7)}$$

Even though the experiment by Strand *et al.* (2006a) was carried out at 100 ℃, the adsorbed amount of sulphate in seawater is much less than the Z^+ value used in the model. This could also be an indication that the anion exchange capacity of 0.2 mol/L PV is too high.

Nevertheless, it is important to mention that the experiment by Strand *et al.* (2006a) was executed at $S_w = 1$, which means that the cores did not contain any crude oil. In the experiments under investigation in this thesis (Puntervold *et al.*, 2015), the cores were initially saturated with $S_w = 0.1$, containing both water and oil. Accordingly, since Z^+ is merely an indication that sulfate is retained, it is possible that sulfate can adhere not only to the chalk surface, but also to other components. Consequently, this could mean that it is reasonable to say that a higher Z^+ value is more representative in a more complex two-phase system.

7.5.3 Temperature

Since carbonate reservoirs varies in temperature, it is very important to understand how the Smart water SI behaves under different conditions. It has been observed in previous work (Zhang & Austad, 2005) that as the reservoir temperature increases, the system will move towards a more water-wet system. The reason is that the acid number of the oil is reduced as the temperature increases due to decarboxylation of the acidic material existing in the oil.

Strand *et al.* (2006a) thoroughly investigated how the adsorption of sulfate on the chalk surface was affected by temperature changes. By exposing the system to different temperatures in a chromatographic wettability test, the authors were able to predict the affinity of sulfate towards the surface. Initially, the cores were 100 % saturated with formation brine containing no SO_4^{2}. Then, the cores were displaced with seawater where the concentrations of SO_4^{2-} and SCN^- were 0.024 mol/L. The results are presented in ***Figure 7.7***.

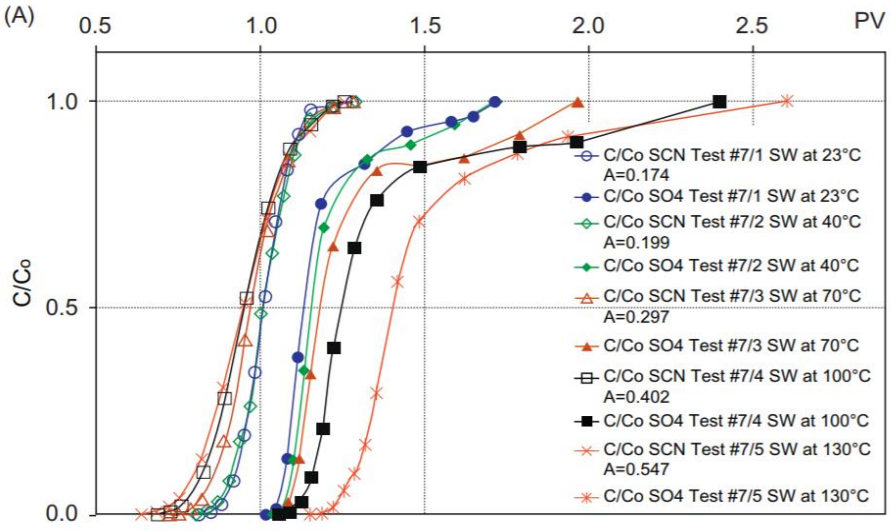

Figure 7.7 *- SO_4^{2-} adsorption at different temperatures taken from Strand et al. (2006a)*

Figure 7.7 indicates that the area between the tracer and SO_4^{2-} increases as the temperature increases. Correspondingly, it is evident that the amount of sulfate adsorbed on the surface increases with higher temperatures. Furthermore, an increase in sulfate adsorption will give a greater efficiency of the wettability alteration process, leading to a higher oil recovery.

To check if the anion exchange model can capture the temperature dependency, three simulations are done by changing the temperature from 90 ℃ to 100 ℃, 110 ℃ and 130 ℃ respectively. All other parameters are kept constant in the model, and the case under investigation is SI of ordinary seawater. The results are shown in ***Figure 7.8*** below.

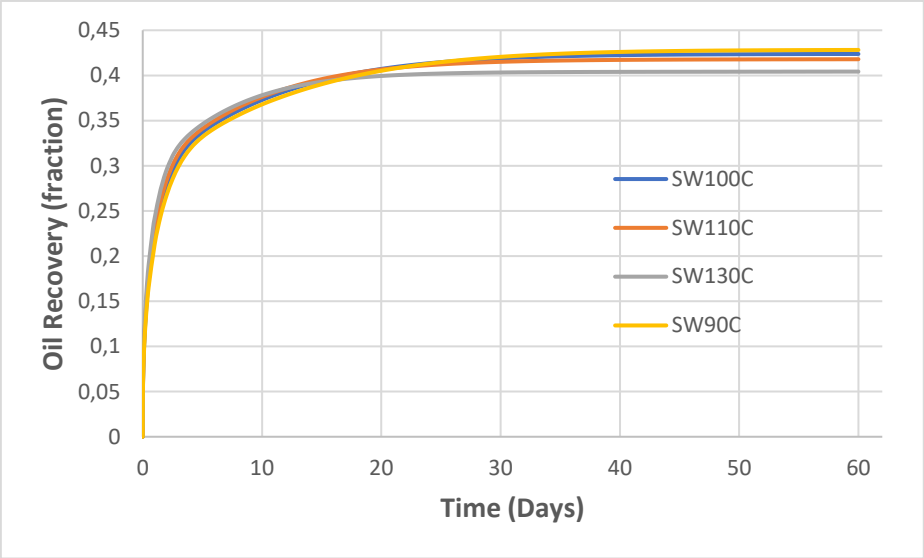

Figure 7.8 *- Simulated SI of ordinary SW at different temperatures*

As is evident in ***Figure 7.8***, the anion exchange model is not able to capture a higher oil recovery as the temperature of the system increases. This can possibly be explained in two different ways. One is that the anion exchange model does not account for other Smart water mechanisms such as precipitation and dissolution of minerals. As the temperature increases, magnesium ions get remarkably reactive due to the splitting of hydrogen bonds as was outlined in *section 3.2.* Accordingly, at higher temperatures, Mg^{2+} will substitute Ca^{2+} at the chalk surface and release oil referring to *eq. 3.1.* Zhang and Austad (2006) also found that dissolution of calcite could be linked to a higher oil recovery, if the process takes place where the organic matter is adsorbed, which was explained in *section 7.3.*

Another explanation is that the anion exchange capacity is set constant in the model. However, based on ***Figure 7.7***, a greater amount of sulfate will adsorb at higher temperatures. Thus, the Z^+ value should be higher at elevated temperatures.

It is also evident in ***Figure 7.8*** that SI of seawater at 130 ℃ has a higher imbibition velocity compared to the cases at lower temperatures. Since SI of ordinary seawater contains sulfate, the model will interpolate between two sets of saturation functions and a too high imbibition velocity could be explained by the diffusion rate of sulfate into the chalk core as outlined in *section 6.4*. The diffusion model implemented in IORCoreSim is directly proportional to the temperature. Thus, at elevated temperatures, the diffusion velocity is higher, which may give a faster imbibition of brines into the core. It also appears from ***Figure 7.8*** that SW130C gives a lower end recovery compared to the other cases. The reason may be due to aqueous complexation reactions referring to *eq. 3.4 – 3.6.* As the temperature increases, free ions in the solution may form complexes, which can contribute to a lower concentration of ions in the imbibing brine. Correspondingly, less sulfate is adsorbed on the chalk surface, leading to a less effective wettability alteration process.

7.5.4 Oil chemistry

Previous work (Hiorth *et al.*, 2010) have shown that the formation- and imbibing brine may influence the charged oil components in the reservoir, especially if there exist several oils with different chemical characteristics. At the oil/water interface, active species such as $-COO^-$, $-COOCa^{2+}$ and $-COOMg^{2+}$ may react with the organic material and cause an increase or reduction in the surface charge. Ions in the solution may also designate complexes with the oil, which in turn could alter the solubility of the organic material.

The current version of IORCoreSim does not include changes in oil chemistry. This means that if the type of oil is varied during the experiments, the model does not capture the chemical variations between the oils. Nevertheless, the experiments under investigation in this thesis (Puntervold *et al.*, 2015) only consider one oil without any changes in oil chemistry.

7.5.5 Calcium concentration

In *section 3.2*, the mechanisms of Smart water SI in carbonates were outlined. Even though SO_4^{2-} acts as a catalyst for the wettability alteration process, the calcium ions are the most important ones in the wettability alteration process. According to Strand and Puntervold (2017), a higher concentration of Ca^{2+} in the FW will give a slightly less water-wet system. This is due to more adsorption of acidic components with increasing amount of calcium ions. Correspondingly, a greater wettability alteration effect is observed under a Smart water SI process in these systems, which corresponds to higher recoveries.

Researchers also believe (Fathi *et al.*, 2011b) that a higher Ca^{2+} concentration in the imbibing brine can contribute to an increased recovery. The reason is that higher calcium activity on the calcite surface causes a larger amount of sulfate adsorption. Correspondingly, a stronger wettability alteration process is generated, and more oil can be retrieved from the core. This theory was also tested by Zhang *et al.* (2006), where different calcium concentrations in the imbibing brine were investigated. They used SK chalk without initial water present, and the SI tests were conducted at 70 ℃ using an oil with AN = 0.55 mg of KOH/g. The results of the study are shown in ***Figure 7.9***.

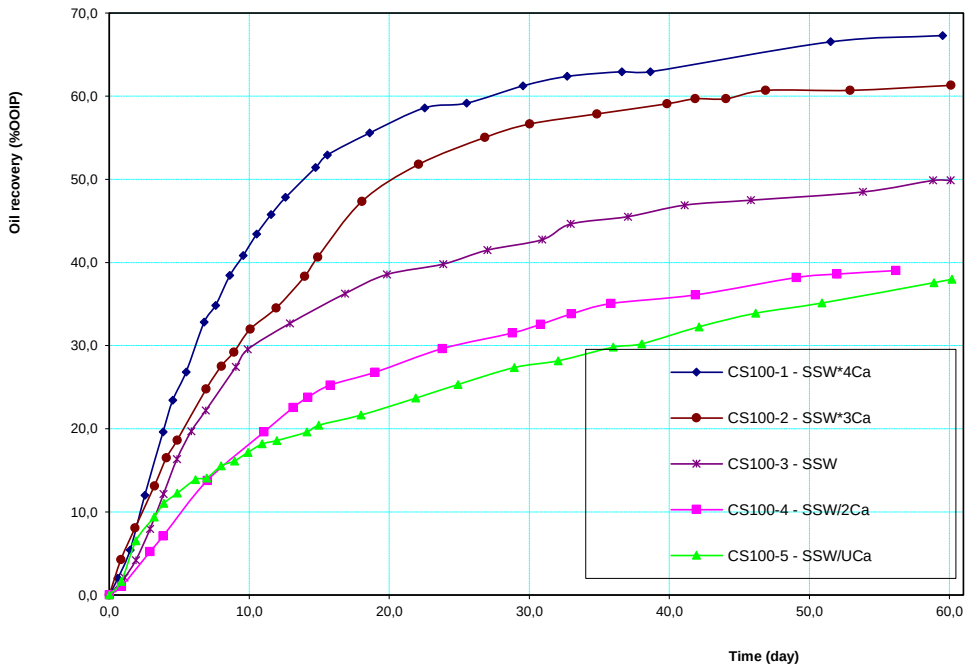

Figure 7.9 *– Oil recovery by SI tests of Ca2+ modified imbibing brines at 70C retrieved from Zhang et al. (2006)*

Even though the temperature and initial water saturation in the tests are different compared to the experiments investigated in this thesis, they are both done on SK chalk with approximately the same oil. It is evident from ***Figure 7.9*** that a higher oil recovery should be achievable when increasing the Ca^{2+} concentration of the imbibing brine. To investigate this observation in the anion exchange model implemented in IORCoreSim, the Ca^{2+} concentration of ordinary SW is changed according to ***Table 7.1***, while the initial water saturation is set equal to 0.001. The imbibing brines are named "SWXCa" where "X" stands for "X" times the Ca^{2+} concentration of ordinary SW. The simulations are run at T=70℃ and the results are given in ***Figure 7.10***.

Table 7.1 *– Ionic composition of imbibing brines with different concentration of Ca2+*

Smart water used				
Ions (mol/L)	**SW**	**SW2Ca**	**SW3Ca**	**SW4Ca**
Na^+	0.450	0.411	0.372	0.333
Ca^{2+}	0.013	0.026	0.039	0.052
Mg^{2+}	0.045	0.045	0.045	0.045
Cl^-	0.525	0.512	0.499	0.486
SO_4^{2-}	0.024	0.024	0.024	0.024
HCO_3^-	0.002	0.002	0.002	0.002
K^+	0.010	0.010	0.010	0.010

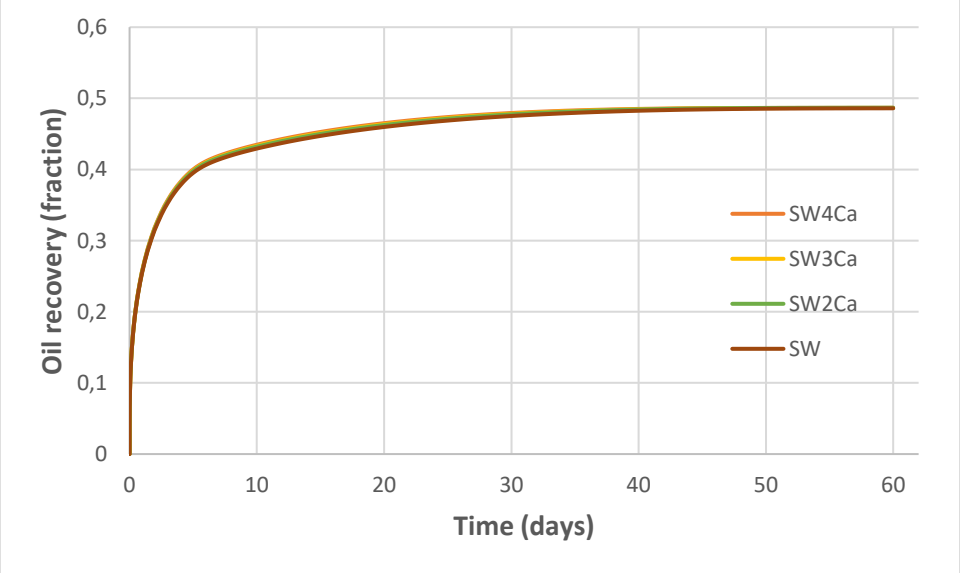

Figure 7.10 *– Simulated SI tests on SK chalk cores at 70C using imbibing brines with different Ca^{2+} concentration*

According to previous experimental research (Fathi *et al.*, 2011b; Zhang *et al.*, 2006), more Ca^{2+} in the system should contribute to a less negative surface, leading to a higher adsorption of sulfate. As is evident in ***Figure 7.10***, the anion exchange model is not able to capture a higher oil recovery as the Ca^{2+} concentration of the imbibing brine increases. Since the SO_4^{2-} concentration is kept constant and equal to the amount present in seawater, the WA and oil recovery follows that of ordinary seawater. The reason could be that the WA mechanism is only linked to the amount of sulfate adsorbed on the chalk surface, which again is directly coupled to the anion exchange capacity of the system. Accordingly, since Z^+ is independent of the calcium concentration, the model will not capture a higher sulfate adsorption as the Ca^{2+} concentration in the imbibing brine increases.

Chapter 8

8 Conclusion and Future work

8.1 Conclusion

The main objective of this thesis was to check if an anion exchange model in IORCoreSim could capture a wettability alteration due to SI of Smart water into chalk cores. Based on the observed results, one can draw the following conclusions:

- The anion exchange model provided a good match between simulated and experimental oil recoveries (Puntervold *et al.*, 2015) by coupling WA to the amount of sulfate adsorbed on the chalk surface.
- The most challenging part of the matching process was to capture the transient behavior of the experiments, rather than the end recoveries. It seems that the oil recovery rate is restricted by the diffusion velocity of sulfate into the core, which could cause problems in larger matrix blocks.
- The model was tested against other experimental data (Zhang *et al.* (2006), Strand et al. (2006a)) to investigate if it had any limitations or shortcomings. The results showed that the model was sensitive to changes in temperature and Ca^{2+} concentration, which could be explained by an independency between the mentioned parameters and Z^{+}.

8.2 Suggestions for Improvements

According to the findings of this thesis, the anion exchange model could be enhanced by improving the implementation of two parameters, namely the diffusion velocity of ions and the ion exchange capacity.

It was assumed that the recovery rate of oil is restricted by the diffusion velocity of sulfate into the core. Even though the diffusion coefficient was reduced, the model was not able to capture the transient behavior of the experiments. The current diffusion model in IORCoreSim (*eq. 6.1)* may be insufficient as it provides too high diffusion rates of ions. Accordingly, a deviation in the time it takes to reach plateau is expected. A suggestion for improvement is to implement a more representative diffusion equation (*eq. 7.3*), with the purpose of providing a better match between experimental and simulated oil recovery rates.

The current anion exchange model did not capture a higher oil recovery at elevated temperatures, nor when the Ca^{2+} concentration of the imbibing brine increased. This could be linked to the independency between the anion exchange capacity, temperature and Ca^{2+} concentration. A suggestion for improvement is to implement Z^{+} as a variable parameter that depends on the concentration of other ions in addition to the temperature of the system.

A more correct approach for modelling the SI of Smart water into carbonate reservoirs could be to include surface complexations. One suggestion is to have a model where the potential determining ions Ca^{2+}, Mg^{2+} and SO_4^{2-} compete against the available surface sites for adsorption. This could solve the problem with diffusion velocity of ions in the system, but the model would be highly complex. Nonetheless, the anion exchange model is a satisfying starting point of modelling SI of Smart water in carbonate reservoirs, and forms a great basis for future work.

References

Abdallah, W., Graue, A., Buckley, J. S., Carnegie, A., Fordham, E., Edwards Bernd Herold, J., Habashy, T., Seleznev, N., Signer, C., Hussain, H., Montaron, B., & Ziauddin, M. (2007). Fundamentals of wettability. *Oilfield Review, 19*(2).

Anderson, W. (1987a). Wettability Literature Survey- Part 4: Effects of Wettability on Capillary Pressure. *Journal of Petroleum Technology, 39*(10), 1283-1300. doi:10.2118/15271-PA

Anderson, W. (1987b). Wettability Literature Survey Part 5: The Effects of Wettability on Relative Permeability. *Journal of Petroleum Technology, 39*(11), 1453-1468. doi:10.2118/16323-PA

Anderson, W. G. (1996). Wettability Literature Survey- Part 1: Rock/Oil/Brine Interactions and the Effects of Core Handling on Wettability. *13932-PA SPE Journal Paper, 38*(10), 1125-2136. doi:10.2118/13932-PA

Austad, T. (2013). *Water-Based EOR in Carbonates and Sandstones: New Chemical Understanding of the EOR Potential Using "Smart Water"*.

Behbahani, H., & Blunt, M. J. (2005). Analysis of Imbibition in Mixed-Wet Rocks Using Pore-Scale Modeling. *Journal of Petroleum Science and Engineering, 10*(04), 466-474. doi:10.2118/90132-PA

Dandekar, A. Y. (2013). *Petroleum Reservoir Rock and Fluid Properties*: Taylor & Francis Inc.

Donaldson, E. C., Thomas, R. D., & Lorenz, P. B. (1969). Wettability Determination and Its Effect on Recovery Efficiency. *Journal of Petroleum Science and Engineering, 9*(01), 13-20. doi:10.2118/2338-PA

Du, H., Lin, X., Xu, Z., & Chu, D. (2015). Electric double-layer transistors: a review of recent progress. *Journal of Material Science, 50*(17). doi:10.1007/s10853-015-9121-y

Evje, S., & Hiorth, A. (2011). A model for interpretation of brine-dependent spontaneous imbibition experiments. *Advances in Water Resources, 34*(12), 1627-1642. doi:10.1016/j.advwatres.2011.09.003

Fathi, S. J., Austad, T., & Strand, S. (2011a). Effect of water-extractable carboxylic acids in crude oil on wettability in carbonates. *Energy & Fuels*, 2587-2592. doi:10.1021/ef200302d

Fathi, S. J., Austad, T., & Strand, S. (2011b). Water-based enhanced oil recovery (EOR) by “Smart Water”: optimal ionic composition for EOR in carbonates. *Energy & Fuels*, 5173-5179. doi:10.1021/ef201019k

Green, D. W., & Willhite, G. P. (1998). Enhanced oil recovery. *6*.

Halling-Sorensen et. al. (1993). Studies in Environmental Science. *54*, 305-336. doi:10.1016/S0166-1116(08)70531-4

Hiorth, A., Cathles, L., & Madland, M. (2010). The Impact of Pore Water Chemistry on Carbonate Surface Charge and Oil Wettability. *Transport in Porous Media, 85*(1), 1-21. doi:10.1007/s11242-010-9543-6

Hiorth, A., Jettestuen, E., Cathles, L. M., & Madland, M. V. (2012). Precipitation, dissolution, and ion exchange processes coupled with a lattice Boltzmann advection diffusion solver. *Geochimica et Cosmochimica Acta, 104*(C), 99-110. doi:10.1016/j.gca.2012.11.019

Høgnesen, E. J. (2005). *EOR in fractured oil-wet chalk. Spontaneous imbibition of water by wettability alteration.* (PhD thesis), UiS,

Jerauld, G. R., & Rathmell, J. J. (1997). Wettability and Relative Permeability of Prudhoe Bay: A Case Study in Mixed-Wet Reservoirs. *SPE Reservoir Engineering, 12*, 58-65. doi:10.2118/28576-PA

Lohne, A. (2013). User's manual for IORCoreSim - combined EOR and SCAL simulator (Version 1.277) Retrieved from IRIS.

Morrow, N. R. (1990). Wettability and Its Effect on Oil Recovery. *Journal of Petroleum Technology, 42*(12), 1476-1484. doi:10.2118/21621-PA

Puntervold, T., Strand, S., & Austad, T. (2007). Water flooding of carbonate reservoirs: Effects of a model base and natural crude oil bases on chalk wettability. *Energy and Fuels, 21*(3), 1606-1616. doi:10.1021/ef060624b

Puntervold, T., Strand, S., Ellouz, R., & Austad, T. (2015). Modified seawater as a smart EOR fluid in chalk. *Journal of Petroleum Science and Engineering, 133*, 440-443. doi:10.1016/j.petrol.2015.06.034

Qiao, C., Johns, R. T., & Li, L. (2016). Modeling Low-Salinity Waterflooding in Chalk and Limestone Reservoirs. *Energy & Fuels, 30*(2), 884-895. doi:10.1021/acs.energyfuels.5b02456

Qiao, C., Li, L., Johns, R. T., & Xu, J. (2015). A Mechanistic Model for Wettability Alteration by Chemically Tuned Waterflooding in Carbonate Reservoirs. *20*(4), 767-783. doi:10.2118/170966-PA

Qiao, Y., Andersen, P. Ø., Evje, S., & Standnes, D. C. (2018). A mixture theory approach to model co- and counter-current two-phase flow in porous media accounting for viscous coupling. *Advances in Water Resources, 112*, 170-188. doi:10.1016/j.advwatres.2017.12.016

Rangel-German, E. R., & Kovscek, A. R. (2002). Experimental and analytical study of multidimensional imbibition in fractured porous media. *Journal of Petroleum Science and Engineering, 36*(1), 45-60. doi:10.1016/S0920-4105(02)00250-4

Salathiel, R. A. (1973). Oil Recovery by Surface Film Drainage In Mixed-Wettability Rocks. *25*(10), 1216-1224. doi:10.2118/4104-PA

Samson, E., Marchand, J., Samson, K. A., Marchand, K. A., & Snyder, K. A. (2003). Calculation of ionic diffusion coefficients on the basis of migration test results. *Materials and Structures/Materiaux et Constructions, 36*(257), 156-165. doi:10.1617/14002

Shariatpanahi, S. F. (2012). *Improved Waterflood Oil Recovery from Carbonate Reservoirs* (PhD), University of Stavanger,

Skjaeveland, S. M., Siqveland, L. M., Kjosavik, A., Thomas, W. L. H., & Virnovsky, G. A. (2000). Capillary Pressure Correlation for Mixed-Wet Reservoirs. *3*(01). doi:10.2118/60900-PA

Standing, M. B. (1974). *Notes on Relative Permeability Relationships*. The Norwegian institute of Technology (NTNU), Norway.

Stiles, J. (2013). *Using special core analysis in reservoir engineering*. Imperical college course notes.

Stoll, M., Hofman, J., Ligthelm, D. J., Faber, M. J., & van den Hoek, P. (2008). Toward Field-Scale Wettability Modification—The Limitations of Diffusive Transport. *11*(03), 633-640. doi:10.2118/107095-PA

Strand, S., Høgnesen, E. J., & Austad, T. (2006a). Wettability alteration of carbonates—Effects of potential determining ions (Ca 2+ and SO 4 2−) and temperature. *Colloids and Surfaces A: Physicochemical and Engineering Aspects, 275*(1), 1-10. doi:10.1016/j.colsurfa.2005.10.061

Strand, S., & Puntervold, T. (2017). *"Smart Water" EOR in Carbonate and Sandstone*. University of Stavanger. Lecture Notes, PET570 "Reservoir Chemistry".

Strand, S., Standnes, D. C., & Austad, T. (2006b). New wettability test for chalk based on chromatographic separation of SCN − and SO42−. *Journal of Petroleum Science and Engineering, 52*(1), 187-197. doi:10.1016/j.petrol.2006.03.021

Thomas, S. (2008). *Enhanced Oil Recovery - An Overview*. Paper presented at the IFP International Conference.

Treiber, L. E., & Owens, W. W. (1972). A Laboratory Evaluation of the Wettability of Fifty Oil-Producing Reservoirs. *12*(6), 531-540. doi:10.2118/3526-PA

Webb, K. J., Black, C. J. J., & Tjetland, G. (2005). *A Laboratory Study Investigating Methods for Improving Oil Recovery in Carbonates*. Paper presented at the International Petroleum Technology Conference, Doha, Qatar.

Xie, X., Weiss, W. W., Tong, Z. J., & Morrow, N. R. (2004). *Improved Oil Recovery from Carbonate Reservoirs by Chemical Stimulation*. Paper presented at the SPE/DOE Symposium on Improved Oil Recovery, Tulsa, Oklahoma.

Yu, L., Evje, S., Kleppe, H., Kårstad, T., Fjelde, I., & Skjaeveland, S. M. (2009). Spontaneous imbibition of seawater into preferentially oil-wet chalk cores — Experiments and simulations. *Journal of Petroleum Science and Engineering, 66*(3), 171-179. doi:10.1016/j.petrol.2009.02.008

Zhang, P., & Austad, T. (2005). *The Relative Effects of Acid Number and Temperature on Chalk Wettability*. Paper presented at the SPE International Symposium on Oilfield Chemistry, The Woodlands, Texas.

Zhang, P., & Austad, T. (2006). Wettability and oil recovery from carbonates: Effects of temperature and potential determining ions. *Colloids and Surfaces A: Physicochemical and Engineering Aspects, 279*(1), 179-187. doi:10.1016/j.colsurfa.2006.01.009

Zhang, P., Tweheyo, M. T., & Austad, T. (2006). Wettability alteration and improved oil recovery in chalk: The effect of calcium in the presence of sulfate. *Energy and Fuels, 20*(5), 2056-2062. doi:10.1021/ef0600816

Zhang, P., Tweheyo, M. T., & Austad, T. (2007). Wettability alteration and improved oil recovery by spontaneous imbibition of seawater into chalk: Impact of the potential determining ions Ca2+, Mg2+, and SO42−. *Colloids and Surfaces A: Physicochemical and Engineering Aspects, 301*(1), 199-208. doi:10.1016/j.colsurfa.2006.12.058

Zhou, X., Morrow, N., & Ma, S. (2000). Interrelationship of Wettability, Initial Water Saturation, Aging Time, and Oil Recovery by Spontaneous Imbibition and Waterflooding. *SPE Journal, 5*(2), 199-207. doi:10.2118/62507-PA